REMOTE SENSING OF SUSPENDED PARTICULATE MATTERS IN LAKE NAIVASHA, KENYA

GIRMA ADERA KEBEDE
February, 2011

SUPERVISORS:
Dr. Ir. Mhd. (Suhyb) Salama
Dr.Ir. C. M. M. (Chris) Mannaerts

REMOTE SENSING OF SUSPENDED PARTICULATE MATTERS IN LAKE NAIVASHA, KENYA

GIRMA ADERA
Enschede, The Netherlands, February, 2011

Thesis submitted to the Faculty of Geo-Information Science and Earth Observation of the University of Twente in partial fulfilment of the requirements for the degree of Master of Science in Geo-information Science and Earth Observation.
Specialization: Water Resources and Environmental Management

SUPERVISORS:
Dr. Ir. Mhd. (Suhyb) Salama
Dr.Ir. C. M. M. (Chris) Mannaerts

THESIS ASSESSMENT BOARD:
Prof. Dr. Ing. (Wouter) Verhoef (Chair)
Prof. Dr. D. M. Harper Department of Biology, Leicester University, UK (External Examiner)

DISCLAIMER
This document describes work undertaken as part of a programme of study at the Faculty of Geo-Information Science and Earth Observation of the University of Twente. All views and opinions expressed therein remain the sole responsibility of the author, and do not necessarily represent those of the Faculty.

ABSTRACT

Suspended particulate matter (SPM) play a major role in controlling pollutant transport, light penetration depth and the retention capacity of inland lakes. This in turn affects the underwater life cycle and ecology and available water in the lake.

In this research Lake Naivasha is selected to study the remote sensing of SPM using MERIS and Landsat data and validated with ground based observations. A semi-empirical algorithm to retrieve suspended particulate matter (SPM) is established and evaluated on MERIS and Landsat ETM+7 data. Calibration of the model with in situ data showed that MERIS bands (708 nm and 778 nm) and Landsat ETM+7 band 3 centred at 660 nm are the most suitable bands for SPM retrieval using the suggested algorithm. Derived values of SPM concentration from MERIS were in a good match to measured concentrations with R^2 being above 0.7 and RMSE bellow 0.34 in a logarithmic scale for MERIS. Better results were obtained when validating the model with and Landsat ETM+7 data with R^2 being above 0.8 and RMSE bellow 0.1 in a logarithmic scale.

This study has shown the capability of single band semi-empirical approach model to retrieve concentration of suspended particulate matters for Lake Naivasha using Landsat ETM+7 images. The algorithm provide therefore a benchmark to process archived Landsat data of the Lake Naivasha and facilities time series analysis of SPM dynamics in the Lake.

Keywords: Suspended particulate matter, remote sensing reflectance, Lake Naivasha

ACKNOWLEDGEMENTS

I thank you Lord! You have been my helper all through the steps of my life and You are honest forever.

My deep appreciation and many thanks go to Dr Ir. Mhd. (Suhyb) Salama who supported and guide me as my first supervisor from the initial proposal to the final phase of my thesis. I would also like to appreciate and thank my second supervisor Dr.Ir. C.M.M. (Chris) Mannaerts whom I was benefiting a lot from his deep knowledge and experience in my study area. I thank all my lecturers and staffs of water resource department of ITC for making a friendly and pleasant environment for the last 18 months of my study period.

In fact, all the field work activities would not be successful without the support of local government authorities, private companies and individuals in Naivasha town. Hence I would like to thank Water Resource office of Naivasha town which helped us in facilitating our work. I sincerely appreciate Prof. David Harper who allows us to work the lab analysis in his private laboratory. All the activities would have been impossible without the laboratory facility we had been provided in Naivasha. I would also like to thank Mrs Sarah Higgen who gave us the access to the Lake Naivasha through her private recreational area, and others who were providing us all the services.

I am grateful for the support of European Space Agency which provides me with the satellite data used in this study.

I thank my classmates and country fellows who make my stay in Enschede an enjoyable and wonderful time. Special thanks to EH group and Naivasha team: Wedi Ghirmai, Obbo Bashana, Nobu, Semantha, Desta, Wondme Yakob and Singora.

Finally, I would like to thank my family whose encouragement and prayer is always with me through out my study. Geniye, I have never felt that I was alone and this is your great effort too. Thank you so much for your moral support and encouragement from distance.

This study is funded by Netherlands Fellowship Program and I would like to thank the Government of the Netherlands who gave me this great opportunity awarding NUFFIC scholarship.

Thank you all and God bless you!

TABLE OF CONTENTS

LIST OF FIGURES

LIST OF TABLES

LIST OF ABBREVIATIONS

Term	Description
SPM	Suspended Particulate Matters
AOPs	Apparent Optical Properties
ENVISAT	Environmental Satellite
EO	Earth Observation
IOCCG	International Ocean Color Coordinating Group
IOP	Inherent optical properties
MERIS	Medium Resolution Imaging Spectrometer
NIR	Near Infra-Red
Rrs	Remote Sensing Reflectance
RS	Remote sensing
TOA	Top of atmosphere
WLR	Water leaving reflectance
PAR	Photo-synthetically active radiation
RMSE	Root mean square error
ETM+	Enhanced Thematic Mapper Plus
ESA	European satellite agency
CDOM	Colored dissolved organic matter
Chl	Chlorophyll
MSS	Multi Spectral Sensor
TM	Thematic Mapper
VIS	Visible
SWIR	Short wave Infra-red
TIR	Thermal infra-red
MWIR	Medium wave infra-red
DN	Digital number
NAP	Non –algae particles
a.m.s.l.	above mean sea level
USGS	United States Geological Survey

LIST OF SYMBOLS

$a(\lambda)$	Bulk absorption coefficient $[m^{-1}]$
$bb(\lambda)$	Bulk backscattering coefficient $[m^{-1}]$
$a_{CDOM}(\lambda)$	Absorption coefficient of Colored Dissolved Organic Matter $[m^{-1}]$
$a_{chl}(\lambda)$	Absorption coefficient of phytoplankton pigment (Chlorophyll-a) $[m^{-1}]$
$a_{SPM}(\lambda)$	Absorption coefficient of suspended particulate matters $[m^{-1}]$
$bb_w(\lambda)$	Bulk backscattering coefficient of water molecules $[m^{-1}]$
$bb_{SPM}(\lambda)$	Bulk backscattering coefficient of suspended particulate matters $[m^{-1}]$
$a_w(\lambda)$	Absorption coefficient of water $[m^{-1}]$
C_{spm}	Concentration of SPM $[mgL^{-1}]$
R^2	Correlation coefficient
$E_d(\lambda)$	Down welling irradiance $[W.m^{-2}\eta m^{-1}]$
π	Mathematical constant Pi (3.141593)
$R_d(\lambda)$	Radiance reflected from the surface of the Spectralon $[Wm^{-2}\eta m^{-1}sr^{-1}]$
$Rrs(\lambda)$	Remote Sensing Reflectance $[sr^{-1}]$
$L_w(\lambda)$	Water leaving radiance $[Wm^{-2}\eta m^{-1}sr^{-1}]$
λ	Wavelength $[nm]$
$Tv(\lambda)$	Diffuse transmittance from the target to the sensor [%]
$\alpha(\lambda)$	Product of backscattering fraction and specific backscattering coefficient of SPM $[m^2g^{-1}]$
$\beta(\lambda)$	The total absorption coefficients of all water constituents except water molecules $[m^{-1}]$

1. INTRODUCTION

Lake Naivasha is Kenya's second largest freshwater, which is the main source of public water supply and irrigation for the people living on the lakeshore, and provides different social economic activities, such as horticulture, flower growing and geothermal power generation (Donia, 1998). Despite the socio-economic advantages of the lake, its water quality is deteriorating through time. It has been studied and reported (World Water forum in 2006) that the lake is losing its natural buffer against the inflow of sediments and nutrients. Harper & Mavuti (2004) indicates that the water quality of Lake Naivasha is affected by the sediment inflow with Malewa river.

Suspended particles in water play the major role in controlling the amount of light that penetrate the water, pollutant transport and reducing the retention capacity of the lake. This in turn affects the underwater life cycle and ecology and available water in the lake. One of the major aspects of suspended particulate matter (SPM) transport is the deposition of sediment at the bed, especially because many contaminants are adsorbed by fine sediment or particulate organic matter and the bottom is a deposit for these contaminants, (Pleskachevsky et al., 2005) it can also transport chemicals and suspended pollutants.

Reliable information on SPM can be achieved using remote sensing data from different sensors. A number of methods have been used and developed by researchers using combined remote sensing data and ground based observations, for example Lindström et al. (1999), Herut et al. (2002), Miller & McKee (2004), Pleskachevsky et al. (2005), Binding et al. (2008), Wang & Lu (2010), Salama & Shen (2010) and Nechad et al. (2010) are to list few of the studies.

In this research remote sensing of SPM concentration of Lake Naivasha is studied using MERIS and Landsat ETM+7 products by calibrating and validating using ground based measurements. The outputs of this research can possibly contribute to the sustainable socio-economic activities of the people of Naivasha and its surrounding in addition to its possible use as data for further research. Local soil conservationist will focus on mechanisms to minimize the sediment inflow from the catchment according to the SPM status of the lake.

1.1. Research problem

Regular in situ measurements of SPM is very much time and labour intensive and difficult to cover the spatial variation in detail. The dynamic nature of inland water bodies requires detail coverage in both spatially and temporally. Remote sensing data can be used for estimation of concentration of SPM and it enables to deal with real time SPM status of water bodies at reasonable spatial coverage. It is not space limited and can be used for remote and inaccessible areas too.

Quantification of SPM using remote sensing data has not been yet done for Lake Niavasha. Some of the studies conducted on water quality problems of the lake to list but not limited to are: Geochemical and physical characteristics of sediments using laboratory analysis of samples (Tarras-Wahlberg et al., 2002); Spatial water quality monitoring and assessment (Munoz Villers, 2002), Spatial analysis of water quality and eutrophication controls (McLean, 2001), and building a dynamic water quality evaluation system by Beltran Bolanos (2001).

Monitoring of SPM which is also contributed from sediment inflow is essential to understand underwater ecology and it is one of the most important keys to characterize water quality of the lake.

1.2. Research Objectives and Questions

To support the water quality studies of Lake Naivasha, exploiting the advantage of remote sensing technology is used in this thesis to estimate the SPM concentration of the lake. The general purpose of this study is to estimate the concentration of SPM from MERIS and Landsat ETM+ data using semi-empirical relationships. In order to arrive at this general objective, the following specific objectives were sited:

- ✓ Develop a model to estimate concentration of SPM from MERIS and Landsat ETM+7 data. The model is calibrated and validated using in-situ data
- ✓ Analyze the data to study spatial variability of SPM concentration of the Lake Naivasha

These objectives are planned to answer the following research questions:

- o Can the use of MERIS and Landsat data gives reliable estimation of SPM of Lake Naivasha?
- o Can it be possible to study the spatial and temporal variation of SPM of Lake Naivasha from MERIS and Landsat?

1.3. Hypothesis

Semi-empirical algorithms can be developed from an appropriate adaptation of analytical model for the estimation of SPM.
MERIS and Landsat data can be used for remote sensing of SPM estimation in Lake Naivasha.

1.4. Thesis structure

This thesis document is structured in chapters with a general introduction on the field and research problems, objectives, question and hypothesis in Chapter 1. A brief literatures review on water quality of remote sensing is given in Chapter 2. The study area and materials used for this research is described in Chapter 3. The approached used to conduct this research is explained in Chapter 4. The results of the study are discussed in detail in Chapter 5. Conclusions and recommendations are given in Chapter 6.

2. LITERATURE REVIEW

2.1. Remote sensing of water quality

Conventional water quality monitoring methods demands high cost and time. It requires elaborate in situ measurements and sequential laboratory analysis. Remote sensing applications have been studied for the past decades to help in the assessment of water quality. Relative cost effectiveness of satellite remote sensing observations of water quality conditions and its fast applicability is demonstrated by Zilioli (1997).

Remotely sensed, geospatial imagery can be utilized for variety of water quality applications including monitoring of suspended particulate matters (SPM), algal blooms and colored dissolved organic matters (CDOM). The development of suitable algorithms and improvement of satellite capability enhances the accuracy and reliability of RS products. Gordon & McCluney (1975) studied the estimation of sunlight penetration in sea and applied on MSS on Earth Resources Technology Satellites (ERTS 1), commonly known as Landsat 1. Ritchie (1985) had used Landsat Multi Spectral Scanner (MSS) to investigate the correlation of MSS band with total solids, suspended matters and chlrophyll-a on surface water. Improved techniques and different alternative approaches have been developed through time in different parts of the world (Durand et al., 2000; Gons et al., 2008; Härmä et al., 2001; Lindström et al., 1999; Nas et al., 2010; Vignolo et al., 2006).

2.2. Atmospheric interference

Remotely operated sensors records radiation reflected or emitted by the target object and surrounding surface. Both the radiation emitted from the Sun and the water leaving reflectance pass through the atmosphere before they reach the satellite level and recorded. As the reflected radiation passes through the atmosphere, it is interfered by diffusion by atmospheric constituents like air molecules and dust particles, and absorbed by atmospheric content of greenhouse gases and water vapour.

Cloud cover over the target surface is another barrier for remote sensors operated in the visible and near infrared spectrum. The radiance measured at satellite level is the total of the reflected radiance from water surface plus all the signals contributed from the atmosphere. Hence, cloud free images should be selected and corrected for atmospheric influence. If partially cloud covered images are used, the area covered by the cloud should be identified or masked out.

2.3. Semi-analytical models for remote sensing of SPM

Semi-analytical models have been developed to link remote sensing reflectance from water surface with inherent optical properties (IOPs) of water (Gordon H. R. et al., 1988; Lee et al., 1999). Remote sensing reflectance can be related to IOPs of water as (Gordon et al., 1975):

$$Rrs(\lambda) \propto \frac{bb(\lambda)}{a(\lambda) + bb(\lambda)}$$

Where: $Rrs(\lambda)$ is the remote sensing reflectance from water surface; $bb(\lambda)$ is bulk backscattering coefficient and $a(\lambda)$ is bulk absorption coefficient of water.

Munday Jr & Alfoldi (1979) have tested linear, logarithmic and non-linear diffuse reflectance models to relate remote sensing reflectance with suspended solids concentration using Landsat MSS 5 data. They have found that diffuse reflectance models (Gordon, 1973; Gordon & Brown, 1973; Gordon et al., 1975; Maul & Gordon, 1975) produces high correlation coefficients and close curve-fitting, and therefore proposes for future Landsat studies of suspended solids concentration.

Gordon (1988) model which was established for the use in open sea waters has been adapted for the use in inland waters. Dekker (1997) has validated the Gordon model for different types of turbid inland waters. Olet (2010) suggests that modifying both empirical and semi analytical models for a specific lake with intensive in situ measurements improves the performance of SPM retrieval from Landsat data.

2.4. Empirical estimation of SPM

Different empirical algorithms have been developed to estimate concentration of SPM from satellite data. Doxaran et al. (2003; 2002) have used band ratio approach to estimate SPM concentrations in highly turbid waters from remote sensing reflectance. As listed in Table2-1, some of the studies like Ritchie et al.(1987) and Ritchie & Cooper (1988) were used a linear relation between pixel values at different bands of Landsat and SPM concentration. The relation was suitable for SPM concentration range of (50 – 200) mg/l. Most of the studies used an exponential function between remote sensing reflectance at near infrared and concentration of SPM.

Table 2-1: Different empirical algorithms developed to estimate SPM of a lake from Landsat data

No.	Author	SPM retrieving algorithm	Area
1	(Ritchie J. C. et al., 1987)	SPM = 9.53 - 1583.37*Band1+4322.21*Bnad3-1184.43*Band4	Moon Lake, Mississippi
2	(Ritchie J. C. & Cooper C. M., 1988)	SPM= - 73.3+ (2029.9 • MSS Band 3) SPM= -124-0-(709.2*MSSBand1) + (1578.3. MSSBand 3)+(1984.0* MSSBand4)	Moon Lake, Mississippi
3	(Jerry C. Ritchie & Cooper, 1991)	Log_e SPM (mg/l) = -9.21(R1/2) + 2.71$(R1/2)^2$ + 8.45	Enid Reservoir in North Central Mississippi
4	(Schiebe et al., 1992)	$R_i = B_i(1\text{-}e(\text{-}SPM/S_i)$	Lake Chicot
5	(Dekker et al., 2002)	TSM=0.7581e61.683Avg(B2.B3)	Lake water

Where: All the algorithms listed in the table are applied on reflectance values of Landsat products. The first three empirical algorithms used different bands of Landsat MSS reflectance values and $R^1/2$ in No.3 is the ratio of MSS band 1 to band 2 reflectance values. B2 and B3 in No.5 are Landsat TM 5 bands 2 and 3. Bi and Si coefficients in No.4 are explained more under 4.3.3.

2.5. SPM remote sensing from MERIS & Landsat

Due to the very dynamic nature of inland water bodies, remote sensing of turbid waters (case 2) requires sensors with high spatial resolution to cover the spatial variation of biological, and physico-chemical properties in fine scale and high spectral resolution to cover the absorption features of chlorophyll (Chl-a) and coloured dissolved organic matter (CDOM).

The Medium Resolution Imaging Spectrometer (MERIS) is one of the remote sensors that are being used to study water optical properties. MERIS is mounted on polar orbiting European Environmental Satellite (ENVISAT) which was launched on 1st of March 2002. It has 15 bands ranging from 412 – 1050 nm with spatial resolution of 300/1200 m. MERIS data has been used to investigate SPM and other water quality parameters in ocean and inland turbid waters. Of which (Chen et al., 2010; Cui et al., 2010; Lee, 2009; Nechad et al., 2010; Salama & Shen, 2010; Shen et al., 2010) are some of those recent studies which applied MERIS data to study SPM concentration.

Landsat ETM+ 7 which was launched in April 1999 is the last series of Landsat mission. The Enhanced Thematic Mapper Plus (ETM+) has 8 bands ranging from 0.45 – 12.5 μm with spatial resolution of 30m (60m-thermal band 6, 15m-panchromatic band 8). Researchers have been using the advantage of high spatial resolution of Landsat data to study SPM concentrations in lake water. Table 2-1 shows some of the studies conducted using Landsat data. The data is also freely available and can be downloaded from online archives.

3. STUDY AREA AND MATERIALS

3.1. Description of study area

3.1.1. General description of Lake Naivasha

Lake Naivasha is located at 0.45ºS latitude and 36.26ºE Longitude. It lies in the Eastern Rift Valley and covers approximately 140 km^2 area. It is one of a series of 23 major lakes in the Eastern Rift Valley – eight in central Ethiopia, eight in Kenya and seven in Tanzania – spanning latitudes from approximately 7º N to 5º S. Lake Naivasha has an altitude of 1890 a.m.s.l. and shallow average depth of about 5m.

Lake Naivasha is the second largest freshwater lake in Kenya. It has been used for agricultural activities including the floriculture industries, residential water supplies, geothermal power plant, and for recreational purposes.

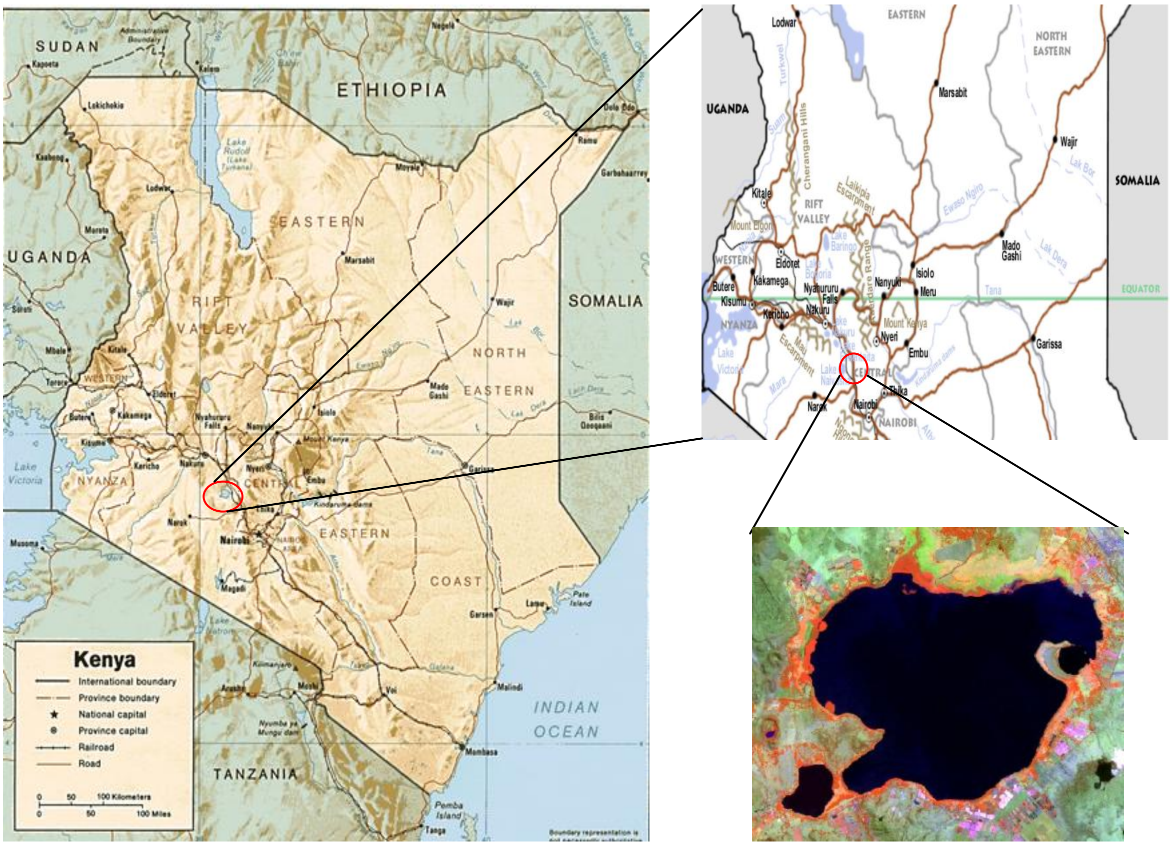

Figure 3-1: Location of Lake Naivasha in Kenya.
Sources: http://www.kenyalogy.com/eng/mapake/mapke.html; Landsat image acquired on 28/05/2000

3.1.2. Climate

The overall climate of the Eastern Rift Valley varies from sub-humid to semi-arid. Lake Naivasha has a mean annual rainfall of about 650mm. The mean temperature around Lake Naivasha is approximately 25^0c with a maximum temperature of 30^0c, with December – March as the hottest period. July is the coldest month with a mean temperature of 23^0c.

3.1.3. Hydrology

Lake Naivasha is a closed system lake. The rivers (Malewa, Gilgil and Karati) drain the surface water from upper catchment area into the lake and the lake has no surface outflow. The watershed area is mainly drained by Malewa and Gilgil rivers with catchment areas of 1700km^2 and 400km^2 respectively. The rivers and ground water sources are a key to the provision of water to the Naivasha and Nakuru municipalities as well as other adjoining human activities. The sediment dynamics of the lake are controlled by the rivers in north and re-suspension of sediments by a wave. The sediments added to the lake by the rivers is transported and deposited in the eastern, central and southern parts of the lake(Tarras-Wahlberg et al., 2002).

3.2. Description of materials used

3.2.1. In situ data

Field campaign was organized from 17th of September up to 3rd of October, 2010. A team of six people were moved and a total of 147 water samples analysis were done and simultaneously radiometric measurements were also recorded at each sampling point locations. Additional radiometric records were also taken on satellite overpass days for the use in atmospheric correction by contrasting with satellite records.

The water samples were taken from the top 10 cm and it is assumed a homogeneous SPM distribution from the top to a depth (Z_{90}) of which 90% of the remote sensing signal comes from. In well mixed lake Z_{90} can be computed from Gordon & McCluney (1975).

Radiometric measurements were carried out from 320nm to 950nm with spectral resolution of 3.33nm using Trios RAMSES-ARC radiance sensor and Trios RAMSES-ACC-VIS irradiance sensor. The irradiance sensor was failed on 27th September 2010 and then radiance from spectralon was measured to compensate the irradiance sensor. The down welling irradiance can be computed from the down welling radiance which is measured as it reflected back from the spectralon.

Figure 3-2: photos from on boat radiometric measurement and laboratory work

3.2.2. Satellite data

MERIS and Landsat ETM+7 satellite data were used for this study. Level 1b MERIS full resolution data were ordered from European Space Agency (ESA). Three cloud free images acquired on 17th, 20th, 23rd, and one partially cloud covered image on 26th of September 2010 were downloaded from ESA's website (http://earth.esa.int). The summary of the obtained satellite data is shown in Table 3-1 below.

Table 3-1: Summary of much up MERIS data

No.	Date of acquisition	Satellite	Sensor
1	17th of September 2010	ENVISAT	MERIS
2	20th of September 2010	ENVISAT	MERIS
3	23rd of September 2010	ENVISAT	MERIS
4	26th of September 2010	ENVISAT	MERIS

MERIS data has 15 bands of which band 1 to band 12 are in visible range and from band13 – band 15 are in Near Infra Red from 400 – 900nm spectral range. MERIS records at ground sampling distance of 300m for full spatial resolution data. MERIS bands are designed to be sensitive to water quality parameters and therefore are suitable to retrieve water quality parameters like colored dissolved organic matter and detritus, suspended particulate matter, and chlorophyll absorption and fluorescence.

Table 3-2: Medium Resolution Imaging Spectrometer (MERIS) bands

Band	Spectral colour	Wavelength (µm)	Bandwidth (nm)	Resolution (m)	Swath Width (km)	Revisit time (days)
Band 1	VIS	0,4125	10	300 (1200)	1150 (575)	3
Band 2	VIS	0,4425	10	300 (1200)	1150 (575)	3
Band 3	VIS	0,49	10	300 (1200)	1150 (575)	3
Band 4	VIS	0,51	10	300 (1200)	1150 (575)	3
Band 5	VIS	0,56	10	300 (1200)	1150 (575)	3
Band 6	VIS	0,62	10	300 (1200)	1150 (575)	3
Band 7	VIS	0,665	10	300 (1200)	1150 (575)	3
Band 8	VIS	0,68125	7,5	300 (1200)	1150 (575)	3
Band 9	VIS	0,70875	10	300 (1200)	1150 (575)	3
Band 10	VIS	0,75375	7,5	300 (1200)	1150 (575)	3
Band 11	VIS	0,76	2,5	300 (1200)	1150 (575)	3
Band 12	VIS	0,77875	15	300 (1200)	1150 (575)	3
Band 13	NIR	0,865	20	300 (1200)	1150 (575)	3
Band 14	NIR	0,885	10	300 (1200)	1150 (575)	3
Band 15	NIR	0,9	10	300 (1200)	1150 (575)	3

Landsat7 ETM+ measures radiance at seven bands: three bands in VIS (Blue-Green, green and red) and the other four bands ranging from NIR to MWIR. All bands have a ground resolution of 30m except for band 6, thermal IR which has 60m resolution.

Table 3-3: Landsat Enhanced Thematic Mapper (ETM+) band configuration

Band	Spectral color	Wavelength range (µm)	Resolution (m)	Swath width (km)	Revisit time (days)
Band 1	VIS	0,45 - 0,515	30	185	16
Band 2	VIS	0,525 - 0,605	30	185	16
Band 3	VIS	0,63 - 0,69	30	185	16
Band 4	NIR	0,76 - 0,9	30	185	16
Band 5	SWIR	1,55 - 1,75	30	185	16
Band 6	TIR	10,4 - 12,5	60	185	16
Band 7	MWIR	2,08 - 2,35	30	185	16

Landsat passes each 16 days and obtaining cloud free match up image was a problem. An image acquired on 28th of September 2010 is found to be cloud free over the lake area though the scene is 48.37% cloud. The image was downloaded from United States Geological Survey's (USGS) online archive (http://edcsns17.cr.usgs.gov/EarthExplorer/order/).

4. METHODS

4.1. Water sample analysis for SPM

Concentration of SPM was determined gravimetrically following Ocean Optics Protocols for Satellite Ocean Color Sensor Validation, Volume 5. 50 to 100ml of water samples were filtered through a pre-weighted 0.45µm Cellulose Nitrate Filters. The filters were washed with distilled water and immediately dried in an oven. The filters were then reweighted using a sensitive electro-balance.

The measured concentration of suspended particulate matters ranges from 1 mg/L to 101 mg/L with a mean value of 34.11 mg/L and standard deviation of 16.6 mg/L.

4.2. Pre-processing of field radiometric measurements

The down welling irradiance and up welling radiance in situ measurements which were recorded at each 10 seconds for a duration of 30 - 40 seconds per a single record were pre-processed prior to computation of remote sensing reflectance. A confidence interval of 95 % was used to average both down welling irradiance and upwelling radiance. For the measurements taken from 28th of September to 3rd of October, 2010, the down welling irradiances were computed from the down welling radiance which was measured as it reflected back from the spectralon. E_d is computed as (D. Doxaran et al., 2004):

$$E_d = \frac{\pi}{R_g} R_d \qquad (1)$$

Where: E_d = the down welling irradiance in $mWm^{-2}nm^{-1}$

R_d = the radiance measurement from the spectralon in $mWm^{-2}Sr^{-1}nm^{-1}$

R_g = the spectalon's bidirectional reflectance function and assumed to be 99% efficient (R_g ~0.99)

The wind speed on the time of measurements was low and the reflectance of skylight from water surface is assumed zero. The remote sensing reflectance was then derived from the averaged values of up welling radiance and down welling irradiance as:

$$Rrs(\lambda) = \frac{L_w(\lambda)}{E_d(\lambda)} \qquad (2)$$

Where:

Rrs = remote sensing reflectance in Sr^{-1}

L_w = water leaving radiance in $mWm^{-2}Sr^{-1}nm^{-1}$ and

E_d = the down welling irradiance just above the water surface in $mWm^{-2}nm^{-1}$

Figure 4-1 shows the remote sensing reflectance computed from the averaged values of Trios RAMSES versus wavelength for all records excluding the outliers described under 4.3.1.

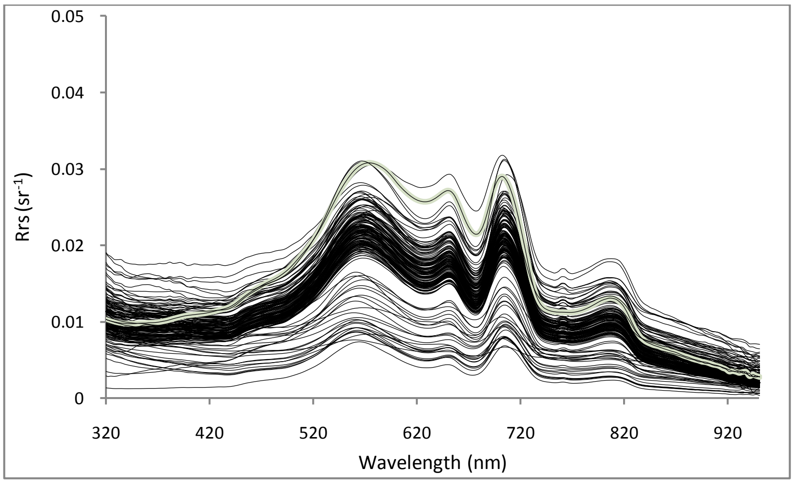

Figure 4-1: Remote sensing reflectance computed from the Trios RAMSES records.

The remote sensing reflectances derived from Trios RAMSES measurements have a spectral resolution of 3.3nm and it was integrated as of Eq. 3 to derive the matching remote sensing reflectance values for MERIS and Landsat ETM+7 sensors.

$$Rrs_I^B = \frac{\int_{\Delta B} Rrs(\lambda)d\lambda}{\int_{\Delta B} d\lambda} \qquad (3)$$

Where: Rrs_I^B is the band integrated remote sensing reflectance computed for each band B with a band width ΔB. Central-wavelength approach is also a good estimation and it has little difference with band weighted values obtained by convoluting the remote sensing values with sensor response functions (Nechad et al., 2010).

4.3. Developing SPM algorithm

4.3.1. Observing relationship between in situ Rrs and SPM measurements

Different regression functions were used to investigate the relation between Rrs at different bands and SPM concentration values. Linear and non-linear regression functions were established for comparison. Figure 4-2 shows radiometric versus logarithm values of SPM concentrations plot of the 147 in situ measurements.

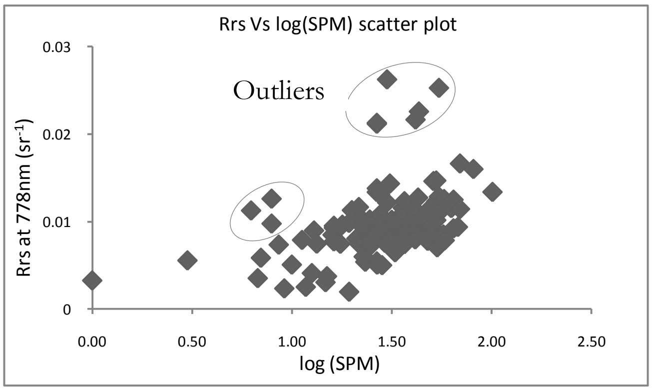

Figure 4-2: Remote sensing reflectance (Rrs) versus logarithm of SPM concentration plot at MERIS band 778nm. The Rrs encircled are outlier values.

Out of the 147 radiometric and SPM concentration measurements, nine outliers were excluded from further analysis. These relatively high values of remote sensing reflectance values could be from floating particles interfering between the instrument and water surface. The 138 Rrs values at 7 MERIS bands were regressed against logarithm of SPM concentrations using 5 different regression functions.

Table 4-1: R^2 values obtained from regressing 138 Rrs measurements and logarithm of SPM concentrations at seven MERIS bands

Regression	MERIS bands in nm						
Functions	560	620	681	708	760	778	865
Exponential	0.41	0.40	0.38	0.43	0.37	0.37	0.25
Polynomial	0.37	0.38	0.36	0.40	0.36	0.36	0.25
Linear	0.37	0.38	0.35	0.40	0.34	0.35	0.22
Logarithmic	0.17	0.16	0.14	0.17	0.13	0.14	0.08
Power	0.2	0.18	0.17	0.21	0.17	0.17	0.12

*The polynomial function is second order polynomial.

As shown in the Table 4-1, the exponential function has relatively higher R^2 values though in general all the regression functions have low R^2 values. The low correlation coefficient between in situ remote sensing reflectance and SPM concentration measurements is possibly due to the different factors that affect the radiometric reading in the field. Such as:

- Instability of the boat during radiometric measurements and hence affecting the angle and direction of radiometric instrument
- Floating algae
- Variation in environmental conditions(like clouds) and
- Manual errors

Due to the above possible factors, different radiometric measurement values were recorded for the same/similar SPM concentration for the same/different days of measurement. Laboratory measurements of SPM concentration is considered to be less susceptible to errors. Very small errors which possibly contributed from manual errors like sampling accuracy were considered to be insignificant.

4.3.2. GSM based semi-empirical Model

The approach adopted and the assumption made in driving the SPM algorithm were based on bio optical modelling and inherent optical properties (IOPs) specific to lake Naivasha. Remote sensing reflectance from water surface can be related to inherent optical properties (Maritorena et al., 2002) as:

$$Rrs(\lambda) = \frac{t}{n_w^2} \sum_{i=1}^{2} g_i \left(\frac{bb(\lambda)}{a(\lambda) + bb(\lambda)} \right)^i \quad (4)$$

Where R_{rs} = remote sensing reflectance; g_1 (=0.0949) and g_2 (=0.0794) are subsurface expansion coefficients due to internal refraction, reflection and sun zenith; t (=0.98) is sea air transmission; and n_w (=1.34) water index of refraction; $a(\lambda)$ and $bb(\lambda)$ are bulk absorption and backscattering coefficients of water column respectively.

The bulk absorption and backscattering coefficients are expressed in terms of optical properties of water (w) and its constituents (SPM, Chl, and CDOM).

$$a(\lambda) = a_w(\lambda) + a_{chl}(\lambda) + a_{SPM}(\lambda) + a_{CDOM}(\lambda) \quad (5)$$

$$bb(\lambda) = bb_w(\lambda) + bb_{SPM}(\lambda) \quad (6)$$

Where: the subscripts w, chl, SPM and CDOM in Eq. (5) refer to the absorption of water molecules, Chlorophyll-a, suspended particulate matter and coloured dissolved organic matter respectively. bb_w and bb_{spm} in Eq. (6) are the backscattering coefficients of water molecules and SPM respectively.

Eq. 5 & 6 can be simplified and re-defined in terms of water constituents and concentration of SPM (C_{spm}) as:

$$a(\lambda) = a_w(\lambda) + \beta(\lambda) \tag{7}$$

$$bb(\lambda) = 0.5b_w(\lambda) + \alpha(\lambda)C_{spm} \tag{8}$$

Where: β [m^{-1}] represents the total absorption coefficients of all water constituents except water molecules. a_w and b_w are the absorption and scattering coefficients of water molecules, and α [m^2g^{-1}] is the product of backscattering fraction and specific backscattering coefficient of SPM.

The values of the absorption coefficients of water molecules are assumed to be constant at a given wavelength and obtained from Pope & Fry (1997). Measurement values by Palmer & Williams (1974) were used for wave length greater than 730nm. Scattering coefficient of water molecules was computed as (Mobley, 1994):

$$b_w = 5.826 \times 10^{-3} \left(\frac{400}{\lambda} \right)^{4.322} \tag{9}$$

The spectral dependency of all terms in Eq. 4 is dropped for brevity. If the absorption and backscattering in Eq. 6 and 7 are function of SPM, then we can solve Eq. 4 to relate with SPM as:

$$Rrs(\lambda) = K\left(\frac{bb_w + \alpha C_{spm}}{bb_w + a_w + \beta + \alpha C_{spm}} \right) \tag{10}$$

Where: K is a constant; the Rrs , bb_w and a_w are described under Equations 4 & 5; C_{spm} is the concentration of suspended particulate matters (SPM); and the fitting coefficients α and β represent the unknowns described under Eq. 7 & 8.

The coefficients α and β varies with wavelength/band and their values were determined from non-linear regression analysis using remote sensing reflectance and SPM data. The model is well-suited to use for wavelengths ≥ 535 nm. Interpolated values were used for bands 560 nm and 681 nm where the model gives negative values.

Table 4-2: Values of α and β interpolated at 10 nm wavelength range

L	β	α	L	β	α
540	150.61	1.43	710	124.13	1.39
560	136.05	1.40	720	152.74	1.41
570	128.76	1.38	730	188.65	1.26
580	121.48	1.37	740	224.56	1.12
590	133.59	1.40	750	235.80	1.10
600	148.51	1.43	760	233.65	1.11
610	161.45	1.43	770	240.62	1.10
620	142.96	1.19	780	236.73	1.11
630	146.84	1.20	790	229.69	1.14
640	143.67	1.22	800	222.06	1.16
650	159.13	1.43	810	221.17	1.17
660	123.77	1.02	820	234.43	1.14
670	130.09	1.09	830	277.61	1.07
680	136.42	1.15	840	305.54	0.97
690	142.75	1.22	850	316.94	0.94
700	124.54	1.39			

The established algorithm was compared with a single band bio-optical algorithm developed by Nechad (2010) to retrieve total suspended matter concentration and with an empirical model (Schiebe et al., 1992). Nechad's single band algorithm is defined as:

$$C_{spm} = A^{p} \frac{\rho_{w}}{1-\rho_{w}/C^{p}} \tag{11}$$

Where

C_{SPM} = Concentration of total suspended matters in g/m^3

ρ_w = reflectance from water surface and

A^P and C^P are calibration constants

V

4.3.3. **Empirical algorithm**

A simple exponential relationship of remote sensing reflectance with concentration of suspended particulate matters (Schiebe et al., 1992) was proposed for this study.

$$Rrs = B(1-e(-C_{SPM}/S_{i}) \tag{12}$$

Where: Rrs is remote sensing reflectance for specific band width; B is the saturation Rrs at very large suspended particulate matters concentration; S_i is suspended sediment concentration at the saturation
The parameters B and S_i were determined by fitting and it varies with change in wave length. At very large SPM concentration, S_i is also approaches very large value and Eq.(12) becomes:

$$Rrs = 0.632 \times B \tag{13}$$

Hence S_i is the suspended sediment concentration at the saturation level constant that is approximately 63% of the saturation reflectance.

4.4. Intercomparision of the three SPM models

The developed GSM based, Nechad and Scheibe models were simulated for ranges of SPM concentrations. The developed model is in general capable of retrieving SPM concentration ranging from low to extremely high values. Figure 4-3 shows GSMBM and Nechad's models fit in all ranges of SPM concentrations. The Schiebe model reaches saturation for SPM concentration beyond 25mg/L. Up to 100 mg/L of SPM concentrations were measured in the field and hence the Scheibe model couldn't be suitable to retrieve higher SPM concentrations for the case of Lake Naivasha.

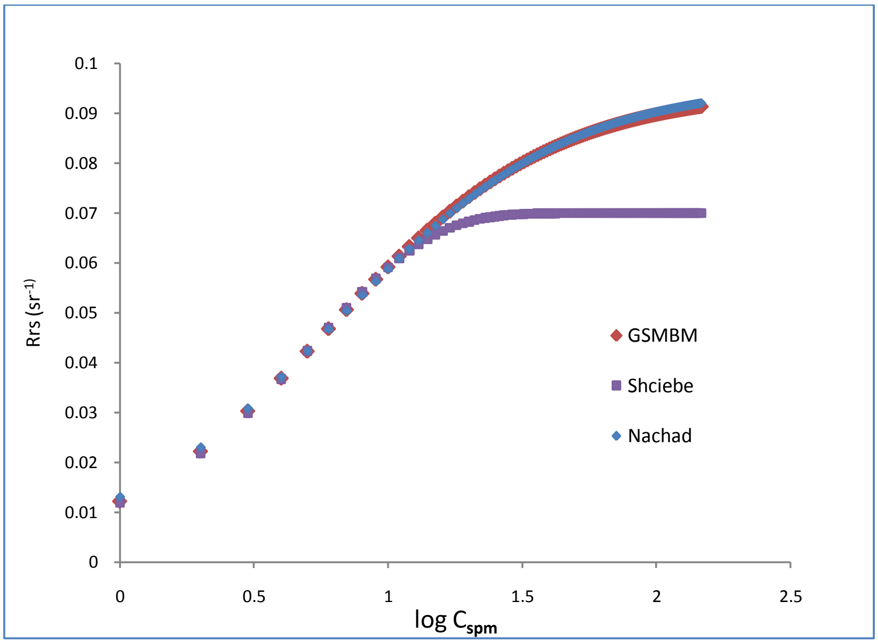

Figure 4-3: Simulation of GSM based model (GSMBM), Nechad's and Scheibe's models

4.5. Calibration of the GSM based model

Non-linear regression analysis was used to obtain the values of the coefficients in Eq. 10 that best fits to the remote sensing reflectance and SPM measurements. The whole in situ data is divided into two data sets. Out of the 138 measurements, the first 70 measurements from 17th – 24th of September 2010 were used as calibration data to derive the coefficients of the established algorithm. The calibration results of both Rrs and SPM concentrations are discussed under 5.3.1 for MERIS and 5.4.1 for Landsat. Figure 4-4 shows calibration of SPM for MERIS band 708 nm.

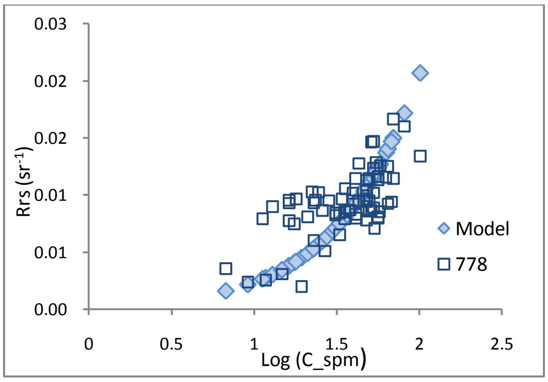

Figure 4-4: GSMB Model Rrs superimposed on 70 Rrs versus logarithm of SPM concentrations for MERIS band 778 nm radiometric characteristics.

4.6. Validation

4.6.1. Validation data set

The model in Eq. 10 was validated for in situ data using the second data set measured from 25th of September to 3rd of October 2010. 68 measurements were used for validating the model. The validation results are discussed under 5.3.2

From the 35 measurements taken on the three MERIS overpass days (20th, 23rd, and 26th of September, 2010), 16 SPM and radiometric measurements taken within +/- 1 hr duration of the overpass time were used for validation of MERIS SPM products. Six match up measurements were used to validate the SPM retrieved from Landsat image acquired on 28th of September 2010.

4.6.2. Measurement site selection for validation of satellite retrieved SPM

According to MERIS lake water validation protocol (Doerffer, 2002) the distance of sampling site from the border of the lake should be >5 km. Though this might not be practical on small lakes, measurement sites used for validation should be at far distance as possible from the shore. This prevents possible effects contributed from the border area. Accordingly measurements taken on the first day, 17th of September were not used as match up data. Match up measurements should also be taken within ± 1 hour of satellite overpass time.

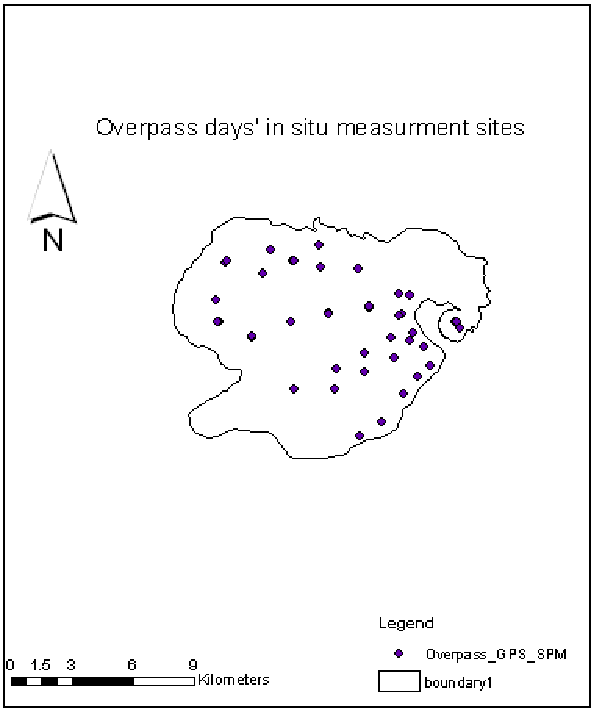

Figure 4-5: Location of all the radiometric measurement and sampling sites on satellite overpass days

4.7. Model performance analysis

Root Mean Square Error (RMSE) and Correlation Coefficient (R^2) statistical analysis parameters were used to evaluate the performance of the model to retrieve the SPM concentration. RMSE was calculated as:

$$RMSE = \sqrt{\frac{\sum \left(Rrs_{measured} - Rrs_{derived} \right)^2}{n}} \tag{14}$$

Where:
$RMSE$ = the root mean square error of remote sensing reflectance in
$Rrs_{measured}$ = the remote sensing reflectance from in situ measurements in
$Rrs_{derived}$ = the remote sensing reflectance derived from the model in and
n = the number of measurements

Eq. 14 was also used to compute RMSE of logarithm of SPM concentrations. The correlation coefficient (R^2) was estimated as:

$$R^2 = \frac{\left(\sum_{j=1}^{n}(Rrs^I - Rrs_m^I)(Rrs^s - Rrs_m^s)\right)^2}{\sum_{j=1}^{n}(Rrs^I - Rrs_m^I)^2(Rrs^s - Rrs_m^s)^2} \quad (15)$$

Where:
Rrs_m^I = the mean in situ remote sensing reflectance and Rrs^I is the jth in situ value
Rrs_m^5 = the mean remote sensing reflectance derived from sensor and Rrs^5 is the jth sensor value
Eq. 15 was also used to calculate the regression coefficient of logarithm of SPM concentrations.

The general procedure of the approach is shown in Figure 4-6 below.

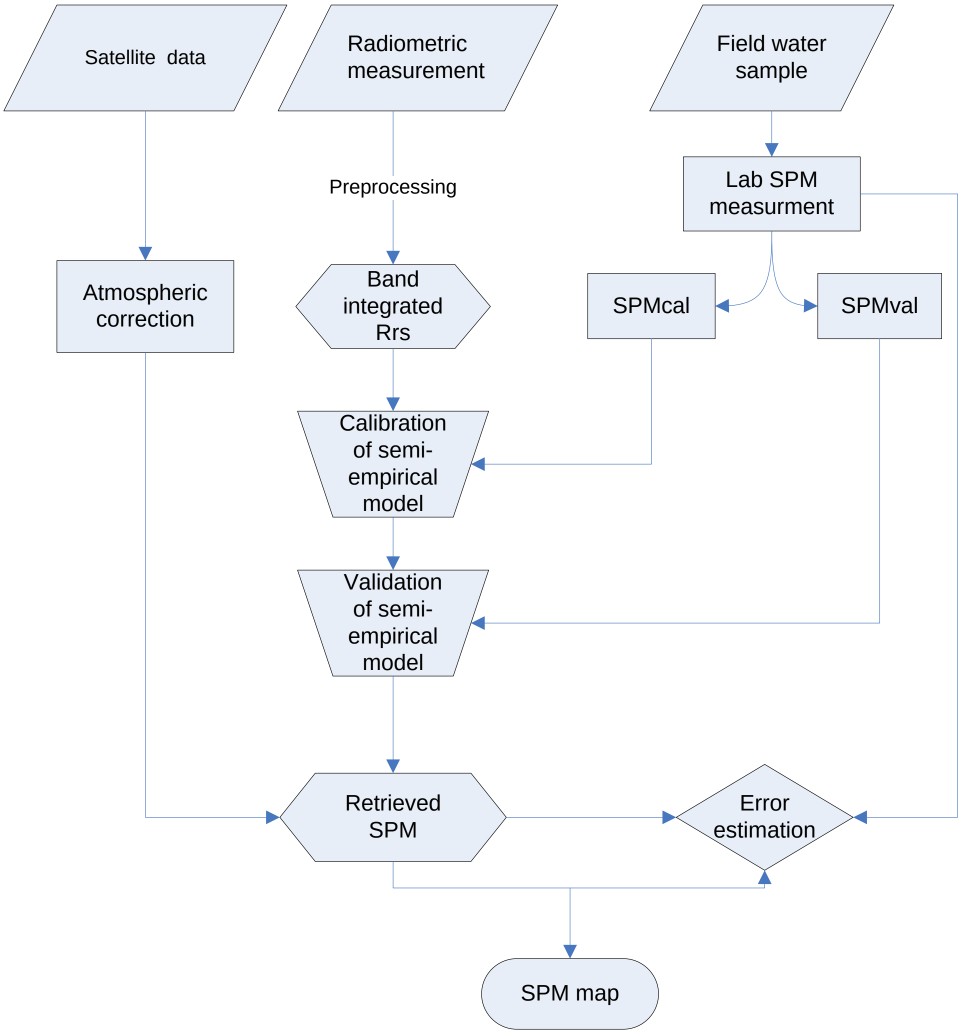

Figure 4-6: Flow chart of the general procedure followed in the methodology

4.8. Satellite data Processing

4.8.1. Conversion of raw digital numbers (DNs) to spectral Radiance

Satellite sensors record digital number assigned for each pixel. This digital number has to be converted to radiance and reflectance values to obtain meaningful information out of the product.

Level 1B MERIS product is radiance data and conversion of DNs to radiance was done for level 1 Landsata ETM+7 data only. Conversion from calibrated $Qcal$ values to spectral radiance L_λ was accomplished with (Chander et al., 2009) equation by knowing the lower and upper limit of the post calibration dynamic range for a specific band. The calibration data in Table A1 are given in the META data of the Landsat image and it can also be obtained from http://landsat.usgs.gov/science_L7_cpf.php

$$L_\lambda = \left(\frac{LMAX_\lambda - LMIN_\lambda}{QcalMAX - Qcal\min} \right)(Qcal - Qcal\min) + LMIN_\lambda \qquad (16)$$

Where

L_λ = Spectral radiance at the sensor's aperture [Wm^{-2} sr^{-1} μm^{-1}]

$Qcal$ = Quantized calibrated pixel value [DN]

$Qcal \min$ = Minimum quantized calibrated pixel value corresponding to $LMIN_\lambda$ [DN]

$Qcal \max$ = Maximum quantized calibrated pixel value corresponding to $LMAX_\lambda$ [DN]

$LMIN_\lambda$ = Spectral at-sensor radiance that is scaled to $Qcal \min$ [Wm^{-2} sr^{-1} μm^{-1}]

$LMAX_\lambda$ = Spectral at-sensor radiance that is scaled to $Qcal \max$ [Wm^{-2} sr^{-1} μm^{-1}]

4.8.2. Conversion of Radiance to remote sensing Reflectance

The spectral radiance calculated in Equation 15 was converted to top of atmosphere (TOA) reflectance using (Chander et al., 2009)equation. TOA reflectance removes the effect of sun elevation angle differences and the eccentricity of the Earth’s orbit. The corrected radiance values of MERIS and Landsat product were converted to reflectance as:

$$Rrs_\lambda = \frac{L_\lambda d^2}{E_\lambda \cos(\theta)} \qquad (17)$$

Where:

Rrs_λ = the remote sensing reflectance [sr^{-1}]

L_λ = Spectral radiance at the sensor's aperture [Wm^{-2} sr^{-1} μm^{-1}]

d = Earth–Sun distance [astronomical units]

E_λ = Mean extraterrestrial solar irradiance [$Wm^{-2}\mu m^{-1}$]

θ = Solar zenith angle [radian]

The solar zenith angle of Landsat can be computed from the sun elevation angle obtained from the META data. The solar zenith angle is 90 minus the sun elevation angle. For the Landsat image obtained on 28th of September 2010, the zenith angle was 90-63.24 =26.76.

The mean exo-atmospheric solar irradiance values of Landsat ETM+7 bands were found from http://landsathandbook.gsfc.nasa.gov/handbook/handbook_htmls/chapter11/chapter11.html as listed per band in Table A1. The corresponding MERIS bands’ values are given in Table 4-3.

Table 4-3: Solar irradiance constant values for each MERIS bands obtained from (http://www.brockmann-consult.de/beam/doc/help/smile/SmileCorrAlgorithmSpecification.html)

Band	Solar Irradiance in $mWm^{-2}nm^{-1}$	Band	Solar Irradiance in $mWm^{-2}nm^{-1}$
412.5	1713.642	708.75	1405.469
442.5	1877.436	753.75	1266.199
490	1929.326	761.875	1249.882
510	1926.839	778.75	1175.723
560	1800.486	865	958.8855
620	1649.71	885	929.7632
665	1530.904	900	895.4086
681.25	1470.226		

4.8.3. **Atmospheric correction of earth observation data**

In situ measurement based atmospheric correction was applied for both MERIS and Landsat images. In situ measured match up remote sensing reflectance values were contrasted with satellite records to estimate path reflectance and air transmittance values.

The signal detected by the sensor is not only from water surface. It is the sum of all sources and remote sensing reflectance from water is a portion of it. The total signal recorded at the sensor level can be described as:

$$Rrs_t(\lambda) = Rrs_r(\lambda) + Rrs_a(\lambda) + Tv(\lambda)(Rrs_{sfc}(\lambda) + Rrs_w(\lambda)) \qquad (18)$$

Where:

Rrs_t is the remote sensing reflectance at the top of the atmosphere; Rrs_r is the Rrs from Rayleigh scattering (air molecules), Rrs_a is the portion from aerosol scattering (in the absence of air molecules), Rrs_{sfc} is the contribution from the water surface, Tv is the diffuse atmospheric transmission and Rrs_w is the desired reflectance of the water. The subscripts represent the contribution from air molecules r, aerosol a, surface sfc, and water w.

Assuming low wind speed during the measurements Rrs_{sfc} becomes very small and can be neglected. The remote sensing reflectance from the water surface can be written as:

$$Rrs_w(\lambda) = \frac{Rrs_t(\lambda) - Rrs_{path}(\lambda)}{Tv(\lambda)} \qquad (19)$$

Where:

$$Rrs_{path}(\lambda) = Rrs_r(\lambda) + Rrs_a(\lambda)$$

The in situ measured remote sensing reflectance from water and the observed Rrs_t from satellite data were substituted in Eq. 18. The atmospheric effect was assumed to be constant over the lake. The $Rrs_{path}(\lambda)$ and $Tv(\lambda)$ were then estimated by solving the set of linear equations (an equation per match up point).

Atmospheric correction of satellite data is summarized in Figure 4-7 below.

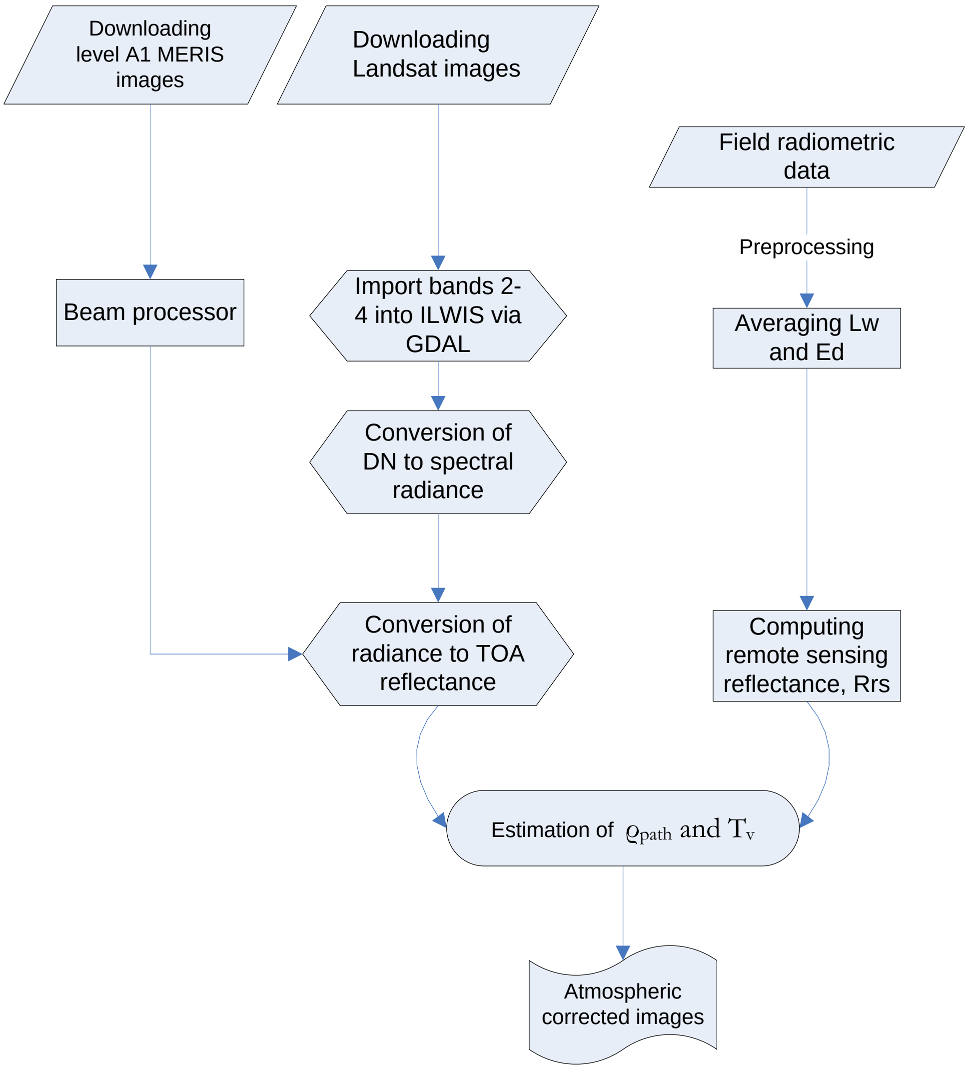

Figure 4-7: Flow chart of atmospheric correction

5. RESULTS AND DISCUSSION

5.1. Radiometric data

Radiometric measurements were taken simultaneously with water sampling and on additional locations during overpass days. The radiometric measurements were carried out based on the IOCCG's ocean optics protocol Volume-4. In general the relationship between the whole in situ remote sensing reflectance and concentration of SPM was low. As shown in Table 4-1 it has a better correlation coefficient of 0.43 for MERIS band 708nm.

The water depth at the radiometric measurement stations were much > 2*Secchi depth which could avoid possible reflection from bottom (Doerffer, 2002). Hence bottom reflection is neglected for the case of Lake Naivasha as it is optically deep water. Studies have also shown that bottom reflectance has an effect on optically shallow water (with low turbidity) for wave lengths in visible ranges. It has very minimum impact and can be neglected for a wavelength range between 740 and 900 nm (Tolk et al., 2000).

5.2. Satelite derived and in situ measured remote sensing reflectance

The remote sensing reflectance values obtained from MERIS and Landsat ETM+7 images were corrected for atmospheric effects following the in situ radiometric measurement based atmospheric correction described under 4.8.3. In situ measured versus satellite derived Rrs scatter plot is shown in Figure 5-1 for MERIS band 708nm. The atmospheric correction results in Table 5-1 shows that satellite derived remote sensing reflectance values are close to the in situ measurements. Correlation coefficient of 0.91 and RMSE of 0.0014sr^{-1} is obtained at MERIS band 708nm, and R^2 of 0.71 & RMSE of 0.0033sr^{-1} at Landsat ETM+7 band 660nm.

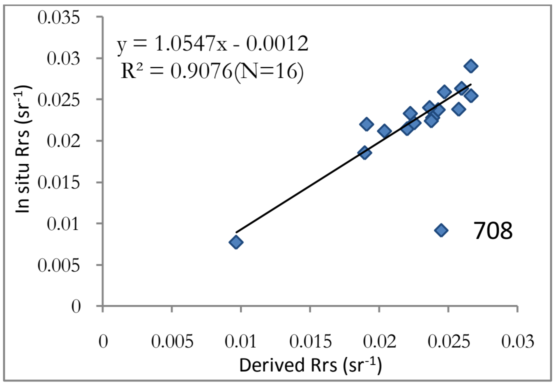

Figure 5-1: In situ MERIS match up remote sensing reflectance measurements versus satellite derived values.

Table 5-1 In situ radiometric measurements based atmospheric correction results for MERIS (a) and Landsat ETM+7 (b) bands

a) Seven MERIS bands' atmospheric correction results

Band in nm	560	620	681	708	762	778	865
R^2	0.90	0.93	0.92	0.91	0.56	0.78	0.68
RMSE	0.0017	0.0012	0.0010	0.0014	0.0025	0.0015	0.0015

b) Atmospheric correction results for three Landsat ETM+7 bands

Band nm	560	660	830
R^2	0.73	0.71	0.00
RMSE	0.0038	0.0033	0.0065

5.3. GSM based model performance on MERIS

5.3.1. Calibration for MERIS radiometric characteristics

The model was calibrated and validated on in situ radiometric and SPM concentration measurements. Suitable bands for the established algorithm were selected according to the performance results of calibration and validation. Bands 560 nm and 865 nm have relatively lower calibration results. MERIS band 760nm is influenced by oxygen absorption and is not suitable for SPM retrieval. Bands 778 nm, 708 nm and 620 nm have relatively better RMSE and R^2 values for the radiometric calibration. While for calibration of the SPM concentrations, bands 708 nm, 778 nm and 681 nm have better RMSE and R^2 comparing with the other bands. The calibration results are shown in Table 5-2 for different MERIS bands.

Table 5-2: Calibration results on radiometric (a) and SPM (b) measurements at 7 MERIS bands
a) Remote sensing reflectance (Rrs)

	560	620	681	708	760	778	865
RMSE	0.0066	0.0048	0.0052	0.0057	0.0030	0.0029	0.0019
R2	0.41	0.43	0.42	0.44	0.43	0.44	0.41

b) SPM concentration

	560	620	681	708	760	778	865
RMSE	0.3816	0.2587	0.1991	0.2850	0.2149	0.2178	0.2015
R2	0.45	0.43	0.43	0.47	0.44	0.45	0.42

In general the algorithm overestimates the SPM concentration values. Very low SPM concentrations are overestimated to large values. There is an overestimation up to more than twice the measured SPM value for lower SPM concentration. The model has produced SPM values with better "root mean square error" for the SPM concentrations above 25 mg/L. The RMSE resulted from calibration for MERIS band 778 nm is shown on Figure 5.2.

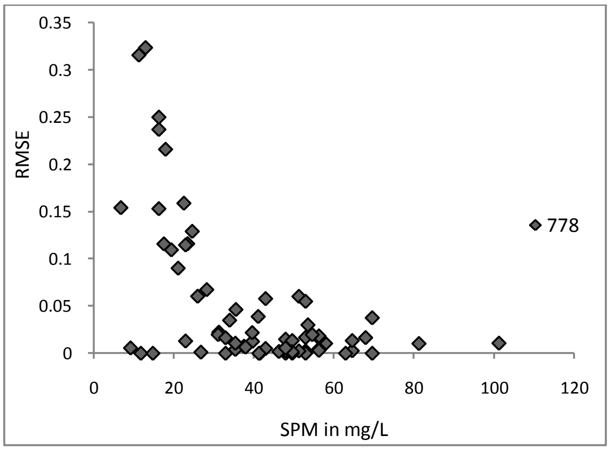

Figure 5-2: The root mean square error of calibration for MERIS band 778nm

Comparing the selected MERIS bands based on the calibration analysis of radiometric and SPM concentration discussed above, band 778 nm has better values of RMSE and R^2 (i.e the calibration fits best at band 778 nm followed by 708 nm).

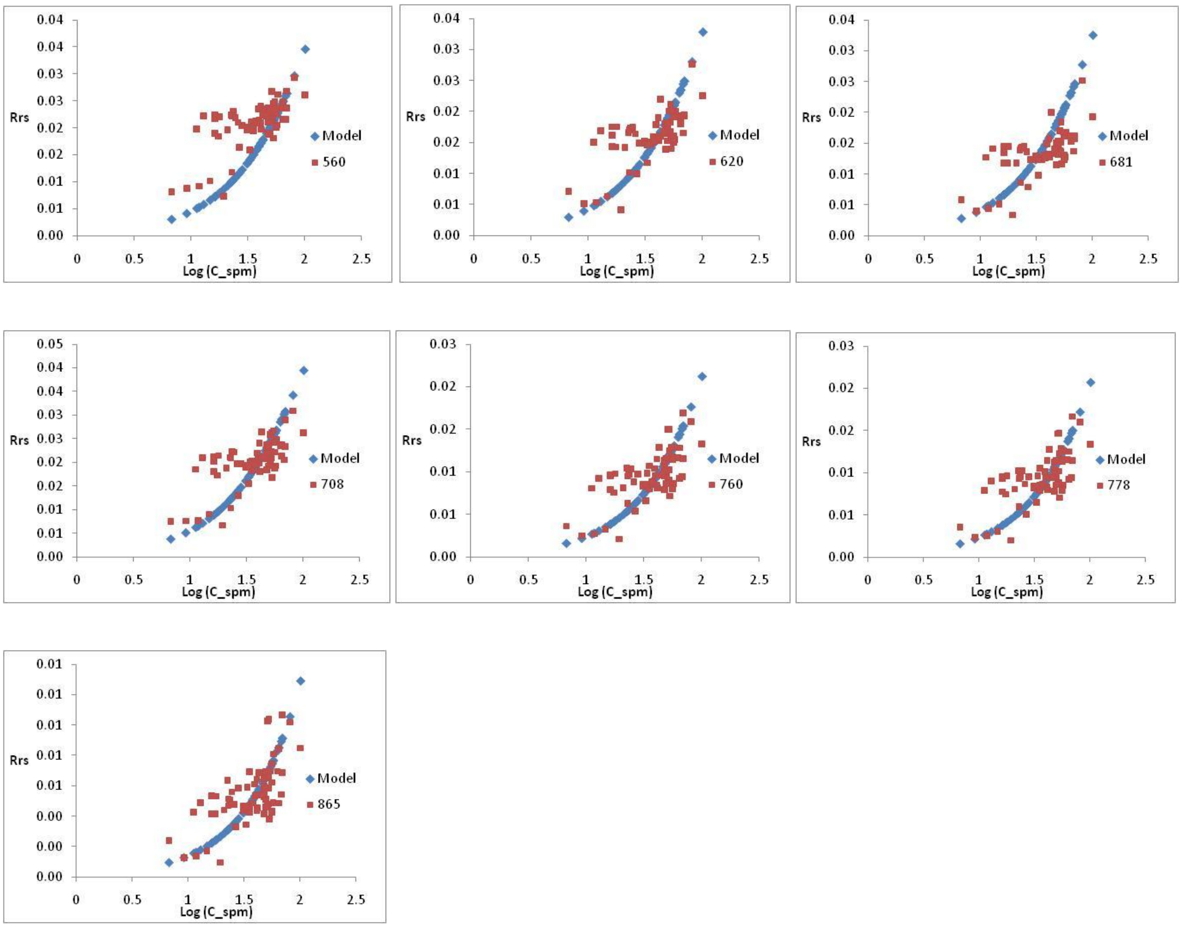

Figure 5-3: The GSM based model Rrs superimposed on 70 in situ Rrs versus SPM concentrations at 7 MERIS bands.

5.3.2. Validation for MERIS spectral characteristics

The model was validated for the second data set of in situ measurements. Bands 681 nm, 620 nm and 708 nm have relatively better RMSE and R^2 value of radiometric validation. Though band 620 nm has the higher R^2 value, it has less calibration performance and higher RMSE of validation than bands 681 nm and 778 nm. Band 681 nm is influenced by absorption of Chlorophyll-a and hence bands 708 nm and 778 nm are suitable bands to use the established algorithm to retrieval SPM from MERIS products. The results of validation are given in Table 5-3

Table 5-3: Validation results of remote sensing reflectance (a) and SPM concentration (b) measurements for selected MERIS bands

a) Remote sensing reflectance

Band	560	620	681	708	760	778	865
RMSE	0.0097	0.0059	0.0041	0.0069	0.0033	0.0034	0.0023
R^2	0.29	0.36	0.33	0.30	0.16	0.19	0.05

b) SPM concentrations

Band	560	620	681	708	760	778	865
RMSE	0.5333	0.3942	0.3129	0.4144	0.3226	0.3319	0.3280
R2	0.42	0.46	0.42	0.42	0.32	0.34	0.13

The derived SPM values are higher than the in situ measurements at all the 7 MERIS bands. The high RMSE values of each band are much influenced by relatively higher overestimation of lower SPM concentrations. Considering for SPM concentrations >10 mg/L as shown in Table 5-4, improves the root mean square error of estimation at all bands.

Table 5-4: Root mean square error values from using all the ranges of SPM concentration used in validation and excluding SPM > 10mg/L

	Band	560	620	681	708	760	778	865
RMSE for	all ranges	0.53	0.39	0.31	0.41	0.32	0.33	0.33
	>10mg/L	0.49	0.34	0.25	0.37	0.25	0.26	0.23

5.3.3. **Satellite estimated SPM using MERIS**

Three match up MERIS images acquired on 20th, 23rd, 26th of September 2010 were used to validate the SPM concentration retrieved from remote sensing products. Based on the results (Table 5-5), Band 778 nm has the best correlation coefficient of 0.73 and RMSE of 0.334 in logarithmic scale.

Table 5-5: Validation results of MERIS SPM product at 5 bands for 17 in situ measurements

Band in nm	560	620	681	708	778
RMSE	0.542	0.397	0.288	0.411	0.334
R2	0.57	0.42	0.44	0.57	0.73

In addition to the lesser validation performance results at 708 nm band, chlorophyll florescence is sensitive at and will probably affect the SPM retrieval using MERIS band 708 nm. Hence band 778 nm will be suitable to retrieve SPM using the established semi-empirical algorithm. Validation results of satellite retrieved SPM using MERIS band 778 nm from the match up images is shown in Figure 5-4.

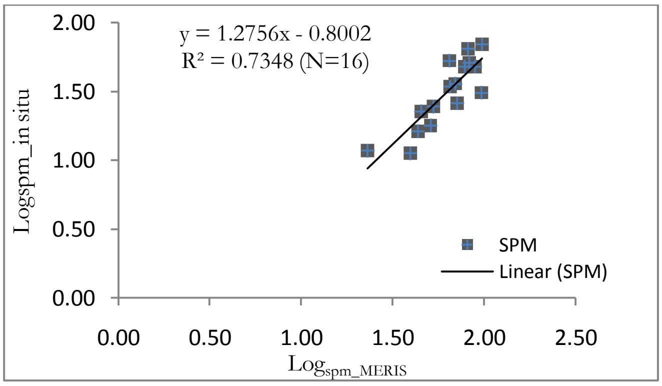

Figure 5-4 In situ versus MERIS retrieved SPM concentrations at band 778 nm

5.4. GSM based model performance on Landsat

5.4.1. Validation for Landsat ETM+7 radiometric characteristics

The established GSM based model is validated with in situ radiometric and SPM measurements and Landsat ETM+7 SPM product. The model's performance was evaluated for three selected Landsat ETM+7 bands. The in situ remote sensing reflectance values were integrated as of Eq. 3 to get the equivalent remote sensing reflectance values for the selected three Landsat ETM+7 bands. The model is then validated with 68 radiometric and laboratory SPM measurements taken from 25th of September to 3rd of October. The validation results for both remote sensing reflectance values and SPM measurements given in Table 5-6 shows that band 3 of Landsat ETM+7 has relatively the best fit and can be suitable to use for retrieval of SPM from Landsat ETN+7 data using the established GSM based model.

Table 5-6: Validation results of radiometric (a) and SPM concentration (b) measurements for three Landsat ETM+7 bands

a) Validation with radiometric measurements

Band(nm)	560	660	830
RMSE	0.0069	0.0052	0.0029
R^2	0.31	0.35	0.13

b) Validation with laboratory SPM measurements

Band(nm)	560	660	830
RMSE	0.4209	0.3573	0.3332
R^2	0.42	0.45	0.25

The root mean square errors of validation results (Table 5-6 and Figure 5-4) show that the model overestimates SPM concentrations as it was also observed for MERIS data. The overestimation is more pronounced in low SPM values and the high RMSE values of each band is much influenced by the much higher RMSE values at lower SPM concentrations. An overestimation of above three times the measured SPM values were observed at lower SPM concentrations.

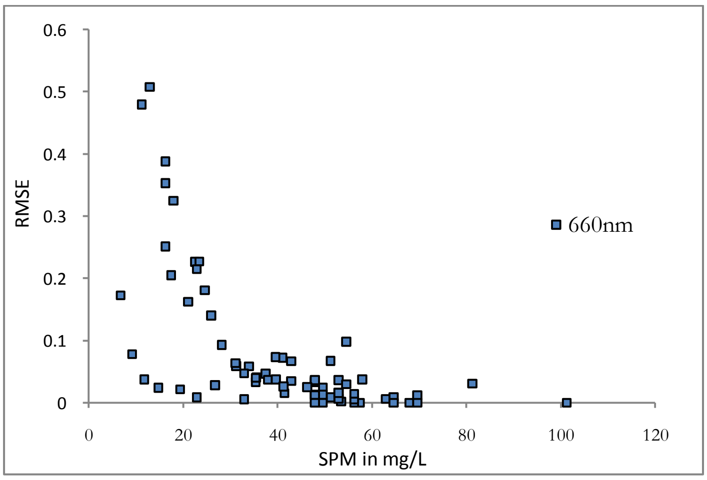

Figure 5-4: The root mean square error of validation for band 3 of Landsat ETM+7 cantered at 660 nm

5.4.2. Satellite estimated SPM using Landsat ETM+7

SPM concentrations were retrieved from Landsat ETM+7 image acquired on 28th of September 2010. The retrieved values were then validated with the match up SPM concentration measurements. Validation of Landsat ETM+7 SPM product with six in situ measurements has remarkable result at band 660 nm. It has a correlation coefficient of 81% and RMSE of 0.08 with the in situ measured SPM concentration in logarithmic scale. The high performance of Landsat retrieved SPM is due to the high spatial resolution capability of Landsat.

Table 5-7: Validation results of Landsat ETM+7 SPM products at three bands

Band in nm	560	660	830
RMSE	0.134	0.081	0.296
R^2	0.74	0.81	0.48

Landsat ETM+7 scenes have data gap since from the failure of Scan Line Corrector (SLC) in 2003. Out of the 10 measurements taken on Landsat overpass day, four measurements lie on the broken line were excluded and six in situ measurements were used for validation of the Landsat ETM+7 SPM product. Five of the measurements were taken from main lake and one from crescent lake. If the measurement taken from crescent lake is excluded, the regression becomes meaningless. The five measurements taken from the main lake has a mean of 39mg/l and standard deviation of 2.24 mg/L and Landsat sensor will not able to differentiate such a small SPM concentration variation. Hence the measurement from the crescent lake should be included and in fact it is measured from crescent lake and not an outlier value.

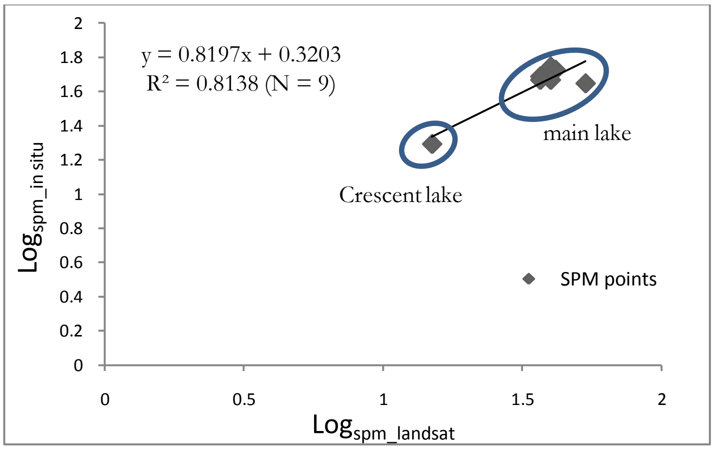

Figure 5-5: In situ SPM measurements versus SPM values retrieved from Landsat ETM+7 on 28th of September 2010.

5.5. SPM map retrieved from satellite

Lake Naivasha catchment is drained by three rivers and these rivers flow into the lake. The inlets of the rivers in the north and northeast shore of the lake are the high SPM spot areas. It has about 60 to 110 mg/L of SPM concentration at the inlet parts of the rivers. SPM maps produced from Landsat ETM+7 and three MERIS images acquired on different days are shown in Figure 5-6 and Figure 5-7.

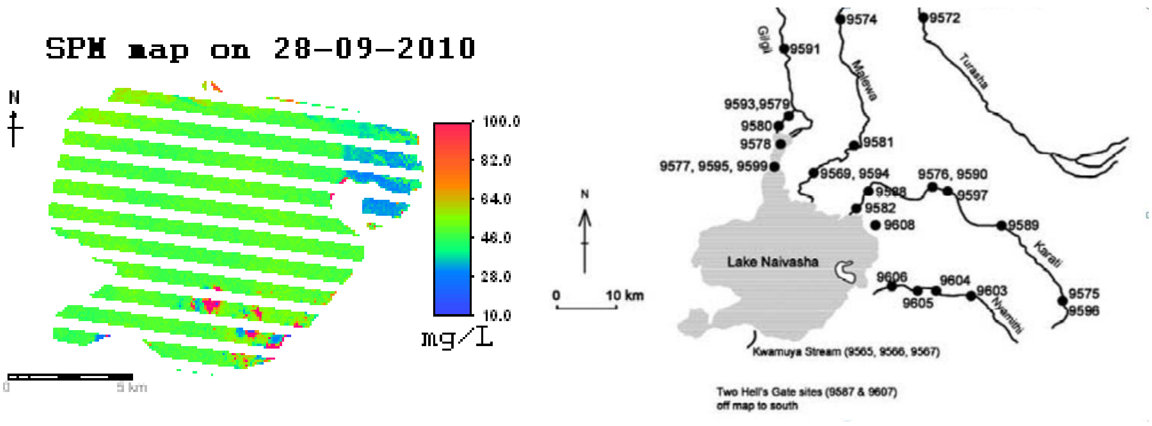

Figure 5-6: (a) SPM map of Lake Naivasha produced from Landsat ETM+7 scene acquired on 28th of September 2010 (b) the three rivers inlet to Lake Naivasha from (Everard et al., 2002)

(a) (b)

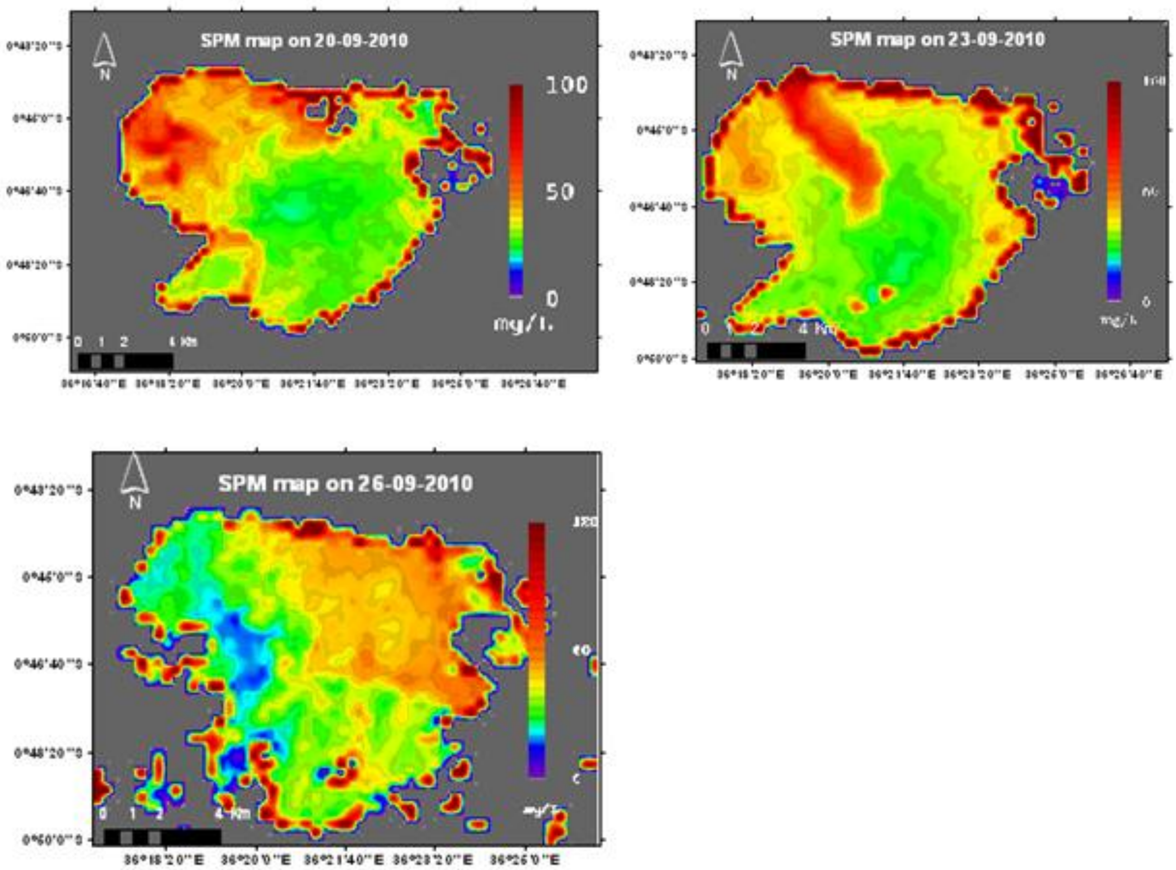

(c)

Figure 5-7: SPM maps of Lake Naivasha produced from MERIS products.

We can observe high concentration of SPM at the north and north western part of the lake (Fig 5-7a). The weather condition was calm at the time of MERIS overpass. High concentration of SPM is expected near the mouth of the three rivers Malewa, Gilgel and Karati. 23rd of September 2010 was proceeded by rain event which has increased discharge of the rivers to the lake. The river's plume can be seen on the MERIS image acquired on 23rd of September 2010. On 26th of September a strong south west wind in the morning time was prevailing with a speed of above 8m/s. This has affected the SPM dynamics in the lake by transporting and re-suspending the sediments at the eastern and north eastern parts of the lake (Figure 5-7c). Floating aquatic plants are also very common on Lake Naivasha. It is transported by wind and wave action and can be seen on both Landsat (Figure 5-6) and MERIS (Figure 5-7) images with high reflectance spot.

5.5.1. **SPM profile**

The SPM profile figure below shows that there is wave effect and re-suspension of SPM in the west and south western part of the lake. The east and south eastern side of the lake has relatively higher SPM concentration and is less affected by re-suspension. This agrees with Tarras-Wahlberg (Tarras-Wahlberg et al., 2002) that the sediment transported into the lake by the rivers is deposited in the eastern, central and southern parts of the lake. Crescent lake is clearer and has lesser SPM concentration than the main lake.

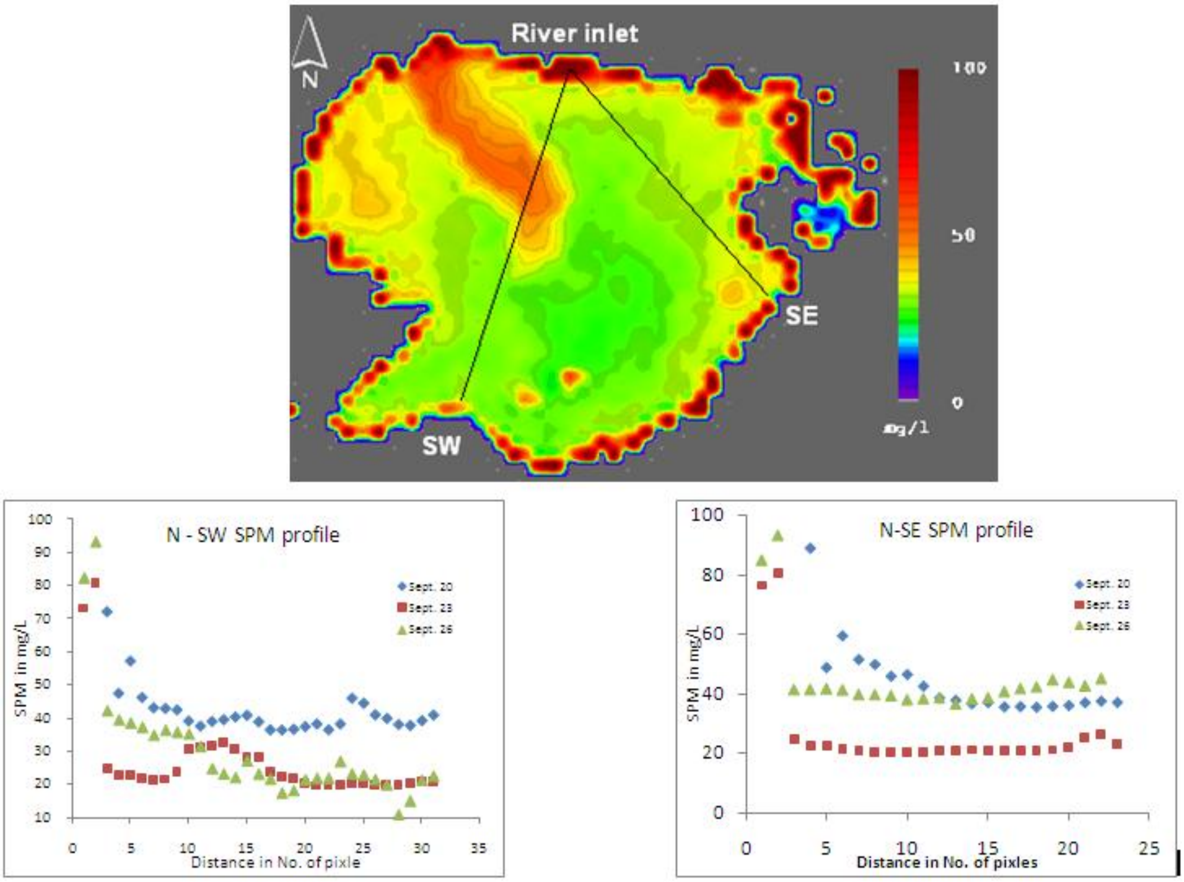

Figure 5-8: SPM profile from the higher concentration of SPM around the inlets of Malewa River (00°43' 56.06S and 36°20'53.43E) to the southwest 0b°48'48.36S & 36°19'43.85 E (a) and southeast (b) at 00°47'21.17 S & 36°23'38.40

6. CONCLUSIONS AND RECOMMONDATIONS

6.1. Conclusions

A semi empirical algorithm has been established in this study to relate the concentration of SPM with a remote sensing reflectance based on the use of single band approach. This algorithm is applied here on MERIS and Landsat ETM+7 data. The algorithm was calibrated and validated using laboratory SPM and remote sensing reflectance computed from in situ measurements. The validation results show that the retrieved SPM concentrations have correlation coefficients of 73% and 81%, and a RMSE of 0.334 and 0.08 in a logarithmic scale respectively for MERIS and Landsat ETM+7 images with the SPM concentration measured in laboratory.

This study has shown that:

- The potential of retrieving SPM concentration of Lake Naivasha from Landsat at a scale of 30m and MERIS at 2-3 days temporal resolution. The established algorithm over estimates low SPM concentrations and it is most suitable to estimate higher SPM concentrations (above 25 mg/L) with relatively lower error of estimation.
- The developed single band semi-empirical algorithm is suitable to retrieve SPM of Lake Naivasha from MERIS and Landsat ETM+7 data. MERIS bands (708 nm and 778 nm) and Landsat ETM+7 band 3 centred at 660 nm are the most suitable bands for SPM retrieval with better results being obtained from Landsat ETM+7.
- Variation of SPM concentrations over Lake Naivasha is also able to be observed on satellite retrieved SPM from both MERIS and a Landsat sensors.
- The dynamic range of SPM in the lake is high and vary in two order of magnitude (1 to 100 mg/l)
- There are some evidences that re-suspension of SPM due to wind leads increase in water turbidity, trap the sediment in opposite direction of the wind.
- The developed algorithm for Landsat provide a benchmark to process archived Landsat data of the Lake Naivasha and facilities time series analysis of SPM dynamics in the Lake.

6.2. Recommendations

Following in situ data observation, the remote sensing reflectance computed from field radiometric records and the laboratory SPM values has low relationships. This might be due to the total effect of the conditions during in situ measurements. Hence taking into consideration of the following recommendations will possibly improve the calibration results.

Though vertically homogeneous water column is assumed on the algorithm, Lake Naivasha water has wave current effect which re-suspend the particles(Tarras-Wahlberg et al., 2002) . This might disturb the homogeneity of the water column and probably contribute to the overestimation of the SPM values by the established algorithm. Water samples should be taken at different depths and integrated for a better value of in situ SPM concentration measurement.

The other practical problem in the field campaign was to wait until the cloud disappears in order to take radiometric measurements. Taking radiometric records under clear sky conditions and less floating particles will possibly improve the calibration performance. Despite the fact that MERIS lake validation protocol (Doerffer, 2002) recommend not to take measurements under such conditions, its realistic that these environmental conditions are highly depend on the season of the area where the lake is situated.

It is hardly possible to keep radiometric instruments in firmed position on unstable and a small boat with manually handled optical device. Hence using relatively stable boat or mounting the device on a fixed platform will fix the problem.

LIST OF REFERENCES

Beltran Bolanos, F. J. (2001). Building a dynamic water quality evaluation system for lake Naivasha Kenya : exploration in the use of DMS. 65.

Binding, C. E., Jerome, J. H., Bukata, R. P., & Booty, W. G. (2008). Spectral absorption properties of dissolved and particulate matter in Lake Erie. [doi: DOI: 10.1016/j.rse.2007.08.017]. *Remote Sensing of Environment, 112*(4), 1702-1711.

Chander, G., Markham, B. L., & Helder, D. L. (2009). Summary of current radiometric calibration coefficients for Landsat MSS, TM, ETM+, and EO-1 ALI sensors. *Remote Sensing of Environment, 113*(5), 893-903.

Chen, X., Lu, J., Cui, T., Jiang, W., Tian, L., Chen, L., et al. (2010). Coupling remote sensing retrieval with numerical simulation for SPM study--Taking Bohai Sea in China as a case. [doi: DOI: 10.1016/j.jag.2009.10.002]. *International Journal of Applied Earth Observation and Geoinformation, 12*(Supplement 2), S203-S211.

Cui, T., Zhang, J., Groom, S., Sun, L., Smyth, T., & Sathyendranath, S. (2010). Validation of MERIS ocean-color products in the Bohai Sea: A case study for turbid coastal waters. [doi: DOI: 10.1016/j.rse.2010.05.009]. *Remote Sensing of Environment, 114*(10), 2326-2336.

Dekker, A. G., Hoogenboom, H. J., Goddijn, L. M., & Malthus, T. J. M. (1997). The relation between inherent optical properties and reflectance spectra in turbid inland waters. *Remote Sensing Reviews, 15*(1), 59-74.

Dekker, A. G., Vos, R. J., & Peters, S. W. M. (2002). Analytical algorithms for lake water TSM estimation for retrospective analyses of TM and SPOT sensor data. *International Journal of Remote Sensing, 23*(1), 15 - 35.

Doerffer, R. (2002). Protocols for the validation of MERIS water products.

Donia, N. S. (1998). Integration of GIS and computer modelling to study the water quality of Lake Naivasha, Central Rift Valley, Kenya. *ITC-MSc-thesis*, 116.

Doxaran, D., Cherukuru, N. C., Lavender, S. J., & Moore, G. F. (2004). Use of a Spectralon Panel to Measure the Downwelling Irradiance Signal: Case Studies and Recommendations. *Appl. Opt., 43*(32), 5981-5986.

Doxaran, D., Froidefond, J.-M., & Castaing, P. (2003). Remote-Sensing Reflectance of Turbid Sediment-Dominated Waters. Reduction of Sediment Type Variations and Changing Illumination Conditions Effects by Use of Reflectance Ratios. *Appl. Opt., 42*(15), 2623-2634.

Doxaran, D., Froidefond, J. M., & Castaing, P. (2002). A reflectance band ratio used to estimate suspended matter concentrations in sediment-dominated coastal waters. *International Journal of Remote Sensing, 23*(23), 5079 - 5085.

Durand, D., Bijaoui, J., & Cauneau, F. (2000). Optical Remote Sensing of Shallow-Water Environmental Parameters: A Feasibility Study. [doi: DOI: 10.1016/S0034-4257(00)00090-0]. *Remote Sensing of Environment, 73*(2), 152-161.

Everard, M., Vale, J. A., Harper, D. M., & Tarras-Wahlberg, H. (2002). The physical attributes of the Lake Naivasha catchment rivers. *Hydrobiologia, 488*(1), 13-25.

Gons, H. J., Auer, M. T., & Effler, S. W. (2008). MERIS satellite chlorophyll mapping of oligotrophic and eutrophic waters in the Laurentian Great Lakes. [doi: DOI: 10.1016/j.rse.2007.06.029]. *Remote Sensing of Environment, 112*(11), 4098-4106.

Gordon H. R., Brown O. B., Evans R. H., Brown J. W., Smith R. C., Baker K. S., et al. (1988). A semianalytic radiance model of ocean color. *J. Geophys. Res, 93*(D9), 10909–10924.

Gordon, H. R. (1973). Simple Calculation of the Diffuse Reflectance of the Ocean. *Appl. Opt., 12*(12), 2803-2804.

Gordon, H. R., & Brown, O. B. (1973). Irradiance Reflectivity of a Flat Ocean as a Function of Its Optical Properties. *Appl. Opt., 12*(7), 1549-1551.

Gordon, H. R., Brown, O. B., & Jacobs, M. M. (1975). Computed Relationships Between the Inherent and Apparent Optical Properties of a Flat Homogeneous Ocean. *Appl. Opt., 14*(2), 417-427.

Gordon, H. R., & McCluney, W. R. (1975). Estimation of the Depth of Sunlight Penetration in the Sea for Remote Sensing. *Appl. Opt., 14*(2), 413-416.

Härmä, P., Vepsäläinen, J., Hannonen, T., Pyhälahti, T., Kämäri, J., Kallio, K., et al. (2001). Detection of water quality using simulated satellite data and semi-empirical algorithms in Finland. [doi: DOI: 10.1016/S0048-9697(00)00688-4]. *The Science of The Total Environment, 268*(1-3), 107-121.

Harper, D., & Mavuti, K. (2004). Ecohydrology to guide the management of a tropical protected area. *Ecohydrology and Hydrobiology, 4*, 287-305.

Herut, B., Kress, N., & Tibor, G. (2002). The use of hyper-spectral remote sensing in compliance monitoring of water quality (phytoplankton and suspended particles) at 'hot spot' areas (Mediterranean coast of Israel). [Proceedings Paper]. *Fresenius Environmental Bulletin, 11*(10A), 782-787.

Lee, Z. (2009). Applying narrowband remote-sensing reflectance models to wideband data. *Appl. Opt., 48*(17), 3177-3183.

Lee, Z., Carder, K. L., Mobley, C. D., Steward, R. G., & Patch, J. S. (1999). Hyperspectral Remote Sensing for Shallow Waters. 2. Deriving Bottom Depths and Water Properties by Optimization. *Appl. Opt., 38*(18), 3831-3843.

Lindström, M., Håkanson, L., Abrahamsson, O., & Johansson, H. (1999). An empirical model for prediction of lake water suspended particulate matter. [doi: DOI: 10.1016/S0304-3800(99)00081-2]. *Ecological Modelling, 121*(2-3), 185-198.

Maritorena, S., Siegel, D. A., & Peterson, A. R. (2002). Optimization of a semianalytical ocean color model for global-scale applications. *Appl. Opt., 41*(15), 2705-2714.

Maul, G. A., & Gordon, H. R. (1975). On the Use of the Earth Resources Technology Satellite (LANDSAT-1) in Optical Oceanography. *Remote Sensing of Environment, 4*, 95-128.

McLean, P. (2001). *Spatial analysis of water quality and eutrophication controls in lake Naivasha Kenya.* ITC, Enschede.

Miller, R. L., & McKee, B. A. (2004). Using MODIS Terra 250 m imagery to map concentrations of total suspended matter in coastal waters. [doi: DOI: 10.1016/j.rse.2004.07.012]. *Remote Sensing of Environment, 93*(1-2), 259-266.

Mobley, C. D. (1994). *Light and water : radiative transfer in natural waters*: San Diego : Academic Press,pp.60.

Munday Jr, J. C., & Alföldi, T. T. (1979). LANDSAT test of diffuse reflectance models for aquatic suspended solids measurement. *Remote Sensing of Environment, 8*(2), 169-183.

Munoz Villers, L. E. (2002). *Spatial water quality monitoring and assessment in Malewa river and Lake Naivasha, Kenya.* ITC, Enschede.

Nas, B., Ekercin, S., Karabörk, H., Berktay, A., & Mulla, D. (2010). An Application of Landsat-5TM Image Data for Water Quality Mapping in Lake Beysehir, Turkey. *Water, Air, & Soil Pollution, 212*(1), 183-197.

Nechad, B., Ruddick, K. G., & Park, Y. (2010). Calibration and validation of a generic multisensor algorithm for mapping of total suspended matter in turbid waters. [doi: DOI: 10.1016/j.rse.2009.11.022]. *Remote Sensing of Environment, 114*(4), 854-866.

Olet, E. (2010). Water quality monitoring of Roxo reservoir using Landsat images and in - situ measurements. In U. o. T. F. o. G.-I. a. E. O. ITC (Ed.) (pp. 76). Enschede: University of Twente Faculty of Geo-Information and Earth Observation ITC.

Palmer, K. F., & Williams, D. (1974). Optical properties of water in the near infrared. *J. Opt. Soc. Am., 64*(8), 1107-1110.

Pleskachevsky, A., Gerhard, G., Jochen, H., & Wolfgang, R. (2005). Synergy of satellite remote sensing and numerical modeling for monitoring of suspended particulate matter. [10.1007/s10236-004-0101-z]. *Ocean Dynamics, 55*(1), 2-9.

Pope, R. M., & Fry, E. S. (1997). Absorption spectrum (380?700 nm) of pure water. II. Integrating cavity measurements. *Appl. Opt., 36*(33), 8710-8723.

Ritchie J. C., & Cooper C. M. (1988). Comparison of measured suspended sediment concentrations with suspended sediment concentrations estimated from Landsat MSS data. *International Journal of Remote Sensing, 9*(3), 379-387.

Ritchie J. C., Cooper C. M., & Yongqing J. (1987). Using landsat multispectral scanner data to estimate suspended sediments in Moon Lake, Mississippi. *Remote Sensing of Environment, 23*(1), 65-81.

Ritchie, J. C., & Cooper, C. M. (1991). Algorithm for estimating surface suspended sediment concentrations with Landsat MSS digital data. *Water Resources Bulletin, 27*(3), 373-379.

Ritchie, J. C., Schiebe, F. R., & Cooper, C. M. (1985). Landsat studies of surface water of Lake Chicot, Arkansas (USA). *Theodolite to satellite. Technical papers 51st annual ASP meeting, Washington, DC, 1985. Vol. 2, (American Society of Photogrammetry, Falls Church, VA)*, 492-498.

Salama, M. S., & Shen, F. (2010). Simultaneous atmospheric correction and quantification of suspended particulate matters from orbital and geostationary earth observation sensors. [doi: DOI: 10.1016/j.ecss.2009.10.001]. *Estuarine, Coastal and Shelf Science, 86*(3), 499-511.
Schiebe, F. R., Harrington Jr, J. A., & Ritchie, J. C. (1992). Remote sensing of suspended sediments: the Lake Chicot, Arkansas project. *International Journal of Remote Sensing, 13*(8), 1487-1509.
Shen, F., Verhoef, W., Zhou, Y., Salama, M., & Liu, X. (2010). Satellite Estimates of Wide-Range Suspended Sediment Concentrations in Changjiang (Yangtze) Estuary Using MERIS Data. *Estuaries and Coasts, 33*(6), 1420-1429.
Tarras-Wahlberg, H., Everard, M., & Harper, D. M. (2002). Geochemical and physical characteristics of river and lake sediments at Naivasha, Kenya. [Article]. *Hydrobiologia, 488*(1-3), 27-41.
Tolk, B. L., Han, L., & Rundquist, D. C. (2000). The impact of bottom brightness on spectral reflectance of suspended sediments. *International Journal of Remote Sensing, 21*(11), 2259 - 2268.
Vignolo, A., Pochettino, A., & Cicerone, D. (2006). Water quality assessment using remote sensing techniques: Medrano Creek, Argentina. *Journal of Environmental Management, 81*(4), 429-433.
Wang, J. J., & Lu, X. X. (2010). Estimation of suspended sediment concentrations using Terra MODIS: An example from the Lower Yangtze River, China. [doi: DOI: 10.1016/j.scitotenv.2009.11.057]. *Science of The Total Environment, 408*(5), 1131-1138.
Zilioli, E., & Brivio, P. A. (1997). The satellite derived optical information for the comparative assessment of lacustrine water quality. *Science of The Total Environment, 196*(3), 229-245.

APPENDICES

Table A 1 Landsat ETM+7 spectral range and calibration ranges

Band Number	Wavelength range	Centerla wavelength	Color in Spectral	Lmin	Lmax	ESUN
Unit	μm	μm		$Wm^{-2}sr\mu m$	$Wm^{-2}sr\ \mu m$	$Wm^{-2}\ \mu m$
1	0.45-0.52	0.485	Blue-green	-6.2	191.6	1997
2	0.52-0.60	0.56	Green	-6.4	196.5	1812
3	0.63-0.69	0.66	Red	-5	152.9	1533
4	0.76-0.90	0.83	Near IR	-5.1	157.4	1039
5	1.55-1.75	1.65	Mid-IR	-1	31.06	230.8
7	2.08-2.35	2.215	Mid-IR	-0.35	10.8	84.9

Table A 13 Landsat retrieved SPM concentrations at three bands corresponding to the measured SPM values taken on the overpass day (28th of September 2010)

Measured SPM		Retrieved SPM		
Site	SPM	B2	B3	B4
S0	15.0	21.41	17.47	11.07
S1	36.7	52.02	44.53	22.79
S3	40.0	56.69	50.86	25.87
S4	41.7	56.69	48.69	22.79
S6	40.0	52.02	41.67	22.79
S9	36.7	49.79	42.52	19.77

Table A 3 MERIS derived SPM concentrations at different bands corresponding to the concentration of SPM measurements taken in the overpass days.

Site no.	Measured SPM	560	620	665	681	708	753	762	778	865
	20/09/10									
1	52.92	86.46	57.70	51.40	43.32	64.98	46.35	46.71	47.48	39.63
2	51.25	127.98	80.77	72.23	60.66	97.31	89.28	90.51	90.60	96.53
3	64.58	109.37	70.62	64.58	53.77	81.96	71.80	72.64	73.16	75.90
4	47.92	98.60	66.96	60.19	50.64	75.88	55.65	56.23	57.63	47.92
5	47.92	100.62	65.91	59.16	49.20	82.33	61.54	62.18	63.94	55.53
6	69.58	129.02	75.81	66.29	53.00	125.18	105.87	107.85	109.45	101.26
7	54.58	174.67	87.90	73.83	57.30	196.14	220.31	227.15	223.57	234.45
8	62.92	99.87	75.49	66.80	56.02	80.28	62.92	62.92	62.92	62.92
9	69.58	100.11	76.88	69.58	56.15	79.54	62.46	63.30	69.58	59.53
10	52.92	94.56	69.64	61.57	51.36	72.71	52.92	52.92	56.17	52.92
11	64.58	84.17	68.11	60.87	51.74	67.71	47.15	47.68	49.88	40.08
12	101.25	121.34	101.25	87.30	74.13	101.25	75.98	76.47	80.49	76.25
13	81.25	157.76	148.80	137.93	119.56	146.09	97.03	98.30	103.61	95.38
	23/09/10									
0	11.75	25.18	14.47	12.50	11.44	16.51	12.07	12.07	11.75	10.62
1	12.92	89.07	61.30	54.01	46.19	65.43	47.49	47.77	48.13	40.59
2	11.25	73.22	51.99	46.58	40.11	53.42	40.68	40.67	41.24	34.77
3	52.92	107.28	88.27	80.57	68.80	100.67	69.48	69.98	71.89	52.92
4	16.25	90.26	65.07	56.45	47.96	66.53	50.65	50.67	51.66	44.32
5	17.92	87.87	65.10	56.52	48.06	68.07	51.26	51.36	52.55	44.27
6	24.58	86.79	64.63	56.71	47.86	72.09	54.66	54.95	56.61	47.00
7	49.58	82.97	68.87	61.05	52.62	65.73	49.58	49.58	49.58	42.66
8	47.92	81.15	62.52	56.66	47.92	70.68	52.96	52.99	54.49	47.92
9	42.92	98.63	94.56	89.22	78.45	101.99	72.29	72.85	75.25	59.59
10	32.92	72.13	49.99	44.81	38.35	55.67	43.71	43.42	44.48	38.20
11	49.58	67.16	52.83	48.15	41.84	56.87	44.05	44.14	45.49	37.86
	26/09/10									
0	12.6	27.17	17.66	15.36	14.36	21.35	19.89	19.83	19.70	21.87
1	27.67	106.19	70.96	62.21	53.19	76.88	59.85	60.16	60.40	56.36
2	31	141.61	97.36	84.70	73.83	93.76	87.81	86.31	88.20	96.69
3	36	111.13	79.71	69.98	59.43	83.68	64.98	65.06	66.03	58.44
4	34.33	99.80	71.56	63.79	54.30	79.07	57.02	56.92	58.27	49.25
5	22.67	93.95	67.74	59.68	50.23	71.11	50.87	50.80	52.45	44.11
6	26	91.48	69.70	62.21	52.95	73.53	54.68	54.51	56.20	47.53
7	19.33	88.57	66.63	59.38	50.55	70.35	52.47	52.38	53.93	45.33
8	16	78.42	57.47	51.19	43.91	59.32	44.04	44.01	44.97	37.87
9	29.33	69.72	48.71	43.25	36.98	50.71	38.54	38.36	39.14	33.64